University of Groningen

Applied Physics

Master thesis

Fluorescence of microdroplets

Author:
Steven van der Veeke

Supervisors:
dr. T.A. (Thomas) Schlathölter
prof. dr. R.P.H. (Rainer) Bischoff

September 16, 2016

Abstract

Electrospray ionization (ESI) is a process where an analyte is transferred to the ionized gas phase. This technique allows fragile molecules, such as most biomolecules, to be transferred to the gas phase and to be characterized with machinery such as mass spectrometers. This process relies on the evaporation and disintegration of small microdroplets, and surprisingly isn't very well understood. This thesis presents an experimental setup that can study microdroplets during the crucial stages of the ESI evaporation process. The theory and working principles of the setup are described as well as the theory of droplet evaporation. The experimental setup relies on a quadrupole ion trap to levitate the droplets in space. The molecular distribution is tracked by making use of fluorescent molecules and a CCD-camera to capture the 2D projections of the fluorescent molecular distributions inside the droplet. The theory needed to reconstruct a 3D distribution from these 2D images is described. The final goal to capture droplets and image the molecular distribution during evaporation is not reached, however an good understanding of the working principles and operation of the experimental setup is used to design a new improved experiment. This new experiment uses an improved quadrupole trap and has several other improvements to study the properties of evaporating droplets.

Contents

Chapter 1

Introduction

"You can know the name of a bird in all the languages of the world, but when you're finished, you'll know absolutely nothing whatever about the bird... So let's look at the bird and see what it's doing – that's what counts. I learned very early the difference between knowing the name of something and knowing something."

— Richard Feynman

This thesis is written to describe an experiment designed to study very small, in the micrometer range, liquid droplets. The aim is to study the internal and external structure of these droplets during the process of evaporation.

Generally at the very basis of research lies the understanding of the processes that are going on. In a broad range of research fields among which not only physics and chemistry, but life sciences and medical science related research fields as well, there is a great interest in structural and molecular information of the samples that are studied. Since the realization that this information of the sample is of fundamental importance for the understanding of the dynamics, researches have been pursuing techniques that give information of the mass and structure of the analyte. Mass spectrometry is a technique which can provide both, the only prerequisite is that the sample needs to be ionized. A mass spectrometer can measure the mass over charge ratio of a sample which gives information about its weight.

Molecules that have been ionized and transferred to the gas phase can be manipulated and fragmented to generate pieces of information that can be combined to unravel the underlying structure. Originally the limitation of this technique was caused by the method of ionization and evaporation of the samples. Before the invention of electrospray ionization, biomolecules could not be brought to the ionized gas phase because of their relative instability. Upon or long before evaporation, the molecules would disintegrate. Up until the late seventies the only techniques used for characterization of biomolecules were electrophoretic, chromatographic or ultracentrifugation methods. These techniques were not very precise and could have an relative error up to 100% [3]. Electrospray ionization, abbreviated as ESI, caused a revolution in the mass spectrometry area because it allowed the investigation of the molecular and structural characteristics of biomolecules.

Not only did ESI proved to be a sensitive and reliable tool for studying these biomolecules, it does not require large amounts of analyte to get reliable results. These characteristics of the technique make ESI very useful in the fields such as biochemistry, pharmacy and medicine where the analyte is usually only available in very low quantities.

Mass spectrometers in combination with ESI can characterize biomolecules without destroying the underlying structure, and therefore this machinery is the most widely used characterization tool in the life sciences [4, 5]. However, the application of this combination of machinery is not only limited to the life sciences, it has found its widespread use in the fields of physics and chemistry to just name a few. Research that aims to study how molecules evolve in time can benefit from the precise analysis that can be done with ESI. Some fine example of the application of ESI is to be found in recent experiments that study the fragmentation and hydrogenation of polycyclic aromatic hydrocarbons molecules. Here the ESI machinery is used to determine the magnitude of both processes [6]. Although this application is very exciting within the field, the most well known applications for the general public lie in the fields of medicine, biology or pharmacy.

1.1 Research

It is indisputable that ESI has had an important role in research of the past years and it is almost certain that it will play the same role in future research. But is should be noted that currently there are some limitations to this technique. In situ measurements have shown differing efficiencies for the mass spectrometer detector. These different results were not only depending on the to be measured molecules (also known as the analyte), but also dependent on the solution used to dissolve this analyte. This implies that some substance comply better with the underlying process of ESI. The technique of ESI is of great importance, and research should be done to improve the sensitivity of the process. We would like to understand the underlying process better and use this understanding to explain why certain substances and solutions perform better than others [7].

Since the discovery of ESI, much research has been done to investigate and improve the results of this technique. ESI relies on the fact that small droplets evaporate and approach a so called 'Rayleigh limit' where the droplets become unstable and undergo fission. By the iterative repetition of this process it ends up with very small droplets containing a few or even a single molecule. Already back in 2003 a publication in Nature has shown that the process of fission is more complicated that was generally thought. Leisner et al. showed that in their experiment the droplets become unstable far before reaching this Rayleigh limit and more interestingly, they captured the whole process of discharge and fission of single droplets by making use of high speed photography.

Leisner et al. captured a microscopic droplets by trapping it in an electrodynamic levitator. They determined the mass/charge ratio in real time by looking at how laser light scattered from the droplet. Figure 1.1 shows the process of disintegration of the microdroplets. It forms sharp tips of jets at the poles of the droplet. They estimated that roughly 100 daughter droplets are formed, which contain approximately 30% of the charge, while only 0.3% of the mass. The break-up mechanism behind this process still remains unclear.

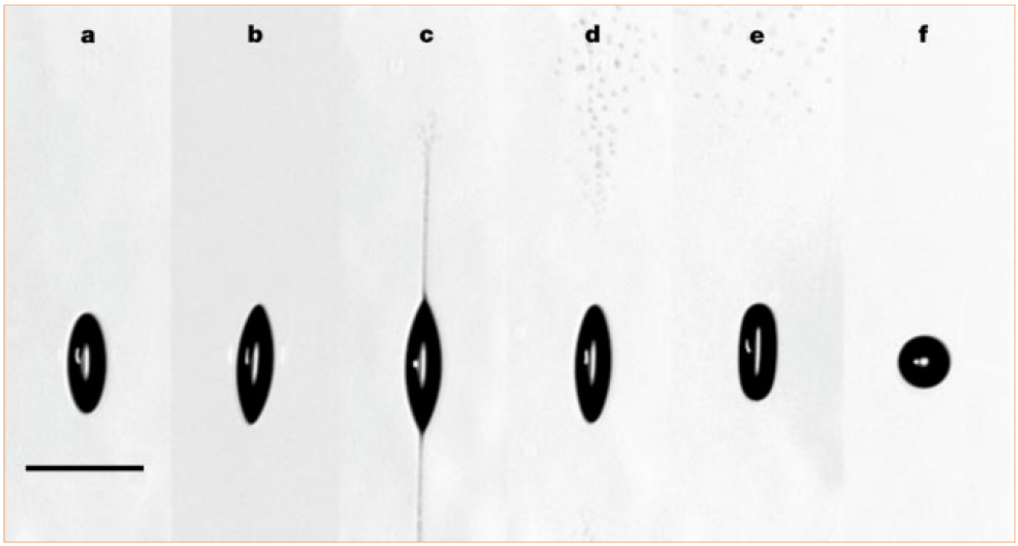

Figure 1.1: Successive microdroplets during the process of disintegration captured by high speed photography. The droplet is roughly 24 μm and is illuminated by a fast flash lamp The difference in time between the first and last picture is 70 micro seconds. We see the droplet forming two sharp tips at the poles, and in picture c a stream of droplets is clearly visible. After this stream of droplets the mother droplets return to its stable round shape, shown in picture f. Image copied from: [8].

Therefore additional research should be done to analyze the behavior of these droplets and develop a better understanding of the break up mechanism. To achieve this it is proposed to study the molecular dynamics of analyte and solution inside the droplets. The initial proposition was to use a high speed camera and trace the cloud of droplets formed by the break up mechanism of ESI. Although not impossible, this would requires the tracking of individual droplets in a relatively huge cloud and imposes limitations on the exact repeatability of a single experiment.

Therefore it is proposed that the experiment should focus on the study of single droplets which can reproduce the exact evaporation path for a large amount of successive droplets. This allows the detailed study for a range of different parameters. This experiment will achieve this by making use of an quadrupole ion trap to maintain individual droplets at a fixed position in space. Knowing how the molecules are distributed inside the droplets during the process of ESI leads to a better understanding of the underlying mechanisms and development of new, more accurate evaporation models. A

renewed and improved understanding can lead to significant improvements. By fine-tuning the machinery and analyte-solution we could be able to improve the overall sensitivity of ESI mass spectrometry.

The main question of this research is:
"How should we design an experiment in which we can study both the shape deformations and molecular distribution within ionized microdroplets during the process of evaporation and disintegration."

Leisner et al. have developed a mathematical description of critically charged microdroplets and found that the deformation path is independent of the density, surface tension and size of the droplets. They suspected that the charge mobility and viscosity have significant impact on the deformation path [9].

Having a setup in which we can measure the shape deformations and molecular distribution of a microdroplet, we can test different droplet parameters that will hopefully shed light on the underlying processes. We could test different molecules among which small, light molecules up to long, heavy molecules. Additionally we could test if we see different behavior for hydrophobic or hydrophilic molecules. And using a variety of solutions to see the influence of surface tension. Most interestingly, we would like to study to which degree the Rayleigh limit is reached for these parameters and compare this with the known studies and models.

To reach this goal we have designed several sub-goals that we need to investigate to come to the above answer:

1. Can we use an quadrupole ion trap to trap and investigate small droplets at a fixed position in space?

2. How can the internal and external movement of molecules inside the droplet be studied during the process of ESI?

3. Can we confirm the known evaporation models with this experimental setup and determine the limits of applicability and limitations for these models?

4. What machinery do we need to study microdroplets with the resolution and detail necessary to unravel the evaporation models?

Chapter 2

Theory

"A single trapped particle floating forever at rest in free space would be the ideal object for precision measurements."

— H. G. Dehmlelt

We want to be able to study the behavior of microdroplets with the application of electrospray ionization in mind. This section explores the theory needed to understand the experiment and the underlying principles. It starts with an explanation of electro spray ionization. This process creates microdroplets which we then want to trap in space using a quadrupole ion trap. To study the molecular distribution inside the droplets we need a marker that can track the movement and presence of analyte. Attaching a fluorescent marker to the analyte allows us to capture the emitted fluorescent photons. By using a CCD-camera we are able to create 2D images of the 3D fluorescent distribution. Using the mathematical theory encapsulated by an Abel transform we can use this 2D image to come up with an radially symmetric 3D distribution. This section will provide the background of above described phenomenons and tools to understand the experiment.

2.1 Electro Spray Ionization [1]

Electrospray ionization is the technique of transferring analyte to the ionized gas phase, leaving the to be studied molecules intact. First ions have to be formed to accommodate the process, secondly the analyte solution goes through a series of steps to transfer the analyte into the ionized gas phase. For convenience we will describe this process by its two main steps:.

Step 1: Production of charged droplets - In figure 2.2 a schematic representation of the ESI apparatus is shown. A metallic capillary which is usually around 0.2 mm o.d. and 0.1 mm i.d. is filled with a mixture of the analyte and a solvent. Then a voltage typical of 2-3 kV is applied between the capillary tip and a counter electrode which is a few centimeters away from this tip. As a result, for these typical parameters, an electric field is formed at the center of the tip of the order of 10^6 V/m.

Due to the electric field charge is accumulated at the tip of the capillary. This increased concentration of charge destabilizes the solution and liquid is drawn out of the tip and forms a so called Taylor cone, which is schematically shown in figure 2.2.

Sir Geoffrey Taylor was the first one to investigate this process and postulated the conditions with respect to the competing forces at play to describe a stable liquid cone, now called the 'Taylor cone' [10]. In ESI the high electric field makes the Taylor cone unstable and an stream of charged droplets, tens of micrometers in diameter are emitted from the capillary tip. At the tip, where this is an continuous process, there needs to be an supply of positive and negative charges. As a source of this charge we will consider the formation of ions. Because only electrons can flow through the metal wire connected to the fluid, electrochemical conversion has to take place to convert ions to electrons. The process at the tip can be seen as an miniature electrolytic cell.

A flow of electrons will be generated as the result of this electrochemical reaction, also known as an oxidation-reduction (redox) reaction. Depending on the polarity it will be an flow to or from the metal capillary tip [11]. If the analyte is not redox active this process is replaced by oxidation and reduction of the solvent for the positive and negative mode respectively [12, 13]. Figure 2.1 shows a table with typical oxidation and reduction reactions for common solvents [14].

Solvent systems	Positive-ion mode Oxidation reactions	E^0 (V)	Negative-ion mode Reduction reactions	E^0 (V)
Water	$2H_2O = O_2 + 4H^+ + 2e^-$	1.23	$2H_2O + O_2 + 4e^- = 4OH^-$	0.40
	$2H_2O = H_2O_2 + 2H^+ + 2e^-$	1.77	$H_2O + O_2^- + e^- = HO_2^- + OH^-$	0.20
	$H_2O = HO^* + H^+ + e^-$	2.72	$H_2O + HO_2^- + e^- = HO^* + 2OH^-$	0.18
			$2H_2O + 2e^- = H_2 + 2OH^-$	0.07
			$2H_2O + O_2 + 2e^- = H_2O_2 + 2OH^-$	−0.13
			$H_2O + O_2 + 2e^- = HO_2^- + OH^-$	−0.83
Methanol	$CH_3OH = HCHO + 2H^+ + 2e^-$	0.23	$CH_3OH + H_2O + 2e^- = CH_4 + 2OH^-$	−0.25
	$CH_3OH + H_2O = HCOOH + 4H^+ + 4e^-$	0.10	$CH_3OH + 2H^+ + 2e^- = CH_4 + H_2O$	0.58
	$HCOOH = CO_2 + 2H^+ + 2e^-$	−0.20		

Figure 2.1: Typical oxidation and reduction reactions that are expected to occur at the capillary tip in electrospray ionization. Table copied from [14].

Typically polar solvents are used (e.g. water, methanol, acetonitrile) because those solvents accommodate the electrochemical reactions easily [14]. When a positive voltage is applied at the capillary tip, the excess of protons formed by the oxidation reaction lead to protonated solvent clusters; $(H_3O^+(H_2O)_n$ for water and $CH_3OH_2^+(CH_3OH)_n$ for methanol) [15]. As a result of the imposed electric field felt at the tip, the positive and negative ions redistribute themselves and drift to and away from the surface of the solution at the tip.

When extracting positive ions, negative ions are created through oxidation of species in the solution at the capillary tip. To maintain equilibrium at the tip interface, the same number of counter ions have to be pumped to the tip, as number of ions are extracted from the tip. Which is provided by continuous oxidation or reduction reactions. Both the oxidation and reduction has been found to occur in the last micrometers of the metallic capillary [3]. The process of oxidation is driven by the lowest oxidation potential which is fully dependent on the solution and its compositions used in ESI. Above method of oxidation reaction was proved by Blades and his group in 1991. They could measure Zn^{2+} ions and Fe^{2+} ions when they used a Zn and a stainless steel capillary tip respectively [12].

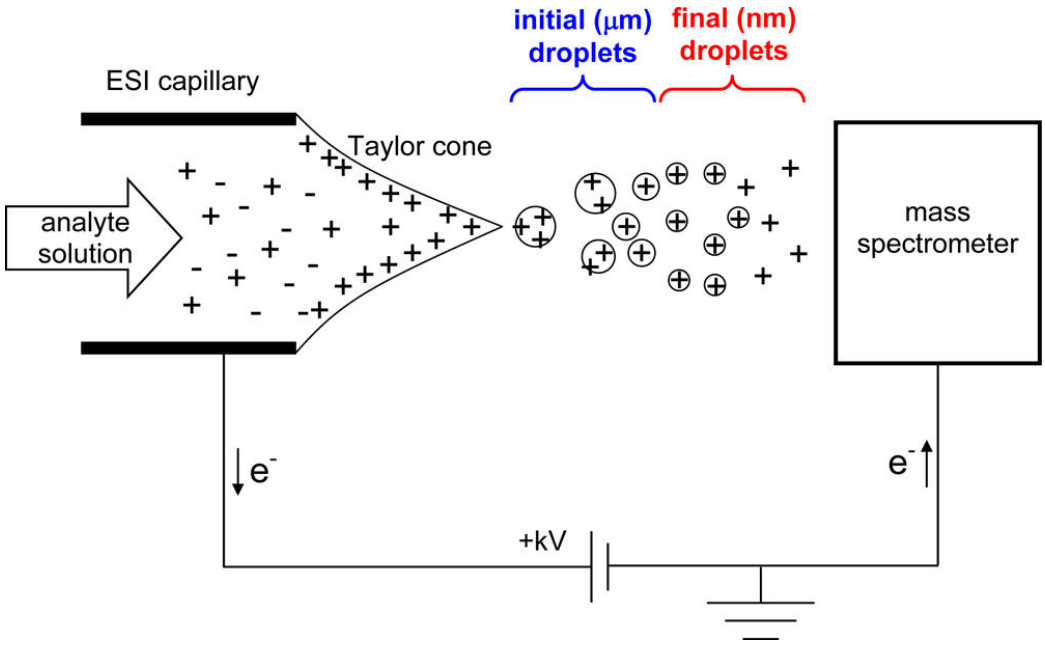

Figure 2.2: A schematic representation of the electrospray ionization process. Image copied from [7].

Step 2: Shrinkage of charged droplets by solvent evaporation - When the droplet is emitted it is typically in the micrometer range (Typically 10 nm, however this size is very solute and capillary dependent [16]). Rayleight found in 1882 that because of the charge in the droplet, the droplets can become unstable when the coulomb repulsion force caused by the ions is equal or larger than the surface tension [17]. This limit where they are exactly equal is now called to Rayleigh limit and is described with the so called fissility parameter X defined as:

$$X = \frac{E_{Coulomb}^{Sphere}}{2E_{surface}^{Sphere}} \tag{2.1}$$

where $E_{Coulomb}^{Sphere}$ and $E_{surface}^{Sphere}$ represent the Coulomb and surface energy of the drop in stable equilibrium. As it turns out this limit is not only applicable for microdroplets, but it has also been shown that this limit is valid for liquid drops of nuclear matter [18].

In practice the Rayleigh limit is never reached and there is a metastable region that starts long before the Rayleigh limit is reached (between X=0.3 and X=1 as described by [19]. Leisner et al. have confirmed this for their experiments with microdroplets of glycol. Already far before reaching the Rayleigh limit

the droplet becomes unstable and will undergo fission. It is generally observed that this fission leads to one relatively large and a number of smaller droplets. It was commonly accepted that the parent droplet emits roughly 2% of its mass in approximately 100 smaller droplets which containing about 15% of its charge [20] but it has been observed by Leisner et al. that this ratio can be up to 0.3% of its mass with 30% of its charge. Due to continuously evaporation of the solvent this is a recursive process in which the droplet becomes so small that the transition to the gas phase of the analyte molecule is possible. A schematic representation of the evaporation and coulomb fission process together with the typical times of these processes is shown in figure 2.3.

Increasing detector response

ESI is mostly used in combination with some kind of detector which always relies on the number of ions that reach this detector. There are a wide range of detector available such as a micro channel plate, or a common mass spectrometer. For example a mass spectrometer detector measures the charge state of the ions, therefore the detector response is directly linked to the electronic charge state of the ions that reach this detector. A mass spectrometer detector measured the mass over charge ration and it should be noted that the electronic results measured by the mass spectrometer detector do not reflect the charge state of the initial analyte, but represents the electrochemical modification (creation of ions) at the probe tip. This electrochemical modification has been tested and results have shown that the applied electric field can have a distinctly different effect on the formation of charged ions. Fenselau and coworkers have shown this by investigating myoglobin at different environmental pH-values [21]. For the myoglobin they concluded that a negative ion spectrum has a better signal to noise ratio than the positive counterpart. This is not necessarily true for other analytes and it should be carefully reevaluated for other experiments.

To understand this we need to know what is happening at the tip. At the tip ions are created through the process of protonation or through the process of deprotonation. The ions are 'pumped out' of this solution because droplets are ejected from the tip, not to be confused with the actual pumping of the fluid through the capillary. In negative mode, this pumping can only be performed if the same number of positive charges are electrochemically neutralized at the tip:

$$(M + zH)^{z+} \qquad protonation \tag{2.2}$$

$$(M - zH)^{z-} \qquad deprotonation \tag{2.3}$$

Protonation is the addition of a proton (H^+) to the solution. Acidification of a solution will result in larger concentrations of H_3O^+ which splits in H_2O and H^+ when it is immersed in a solution which in turn accommodates the protonation process. It is known that protons have higher electrochemical mobility. Adding an acid to the solution can improve the number of ions reaching the detector due to the increased concentration of negative ions because positive charges in the tip are electrochemically neutralized [3].

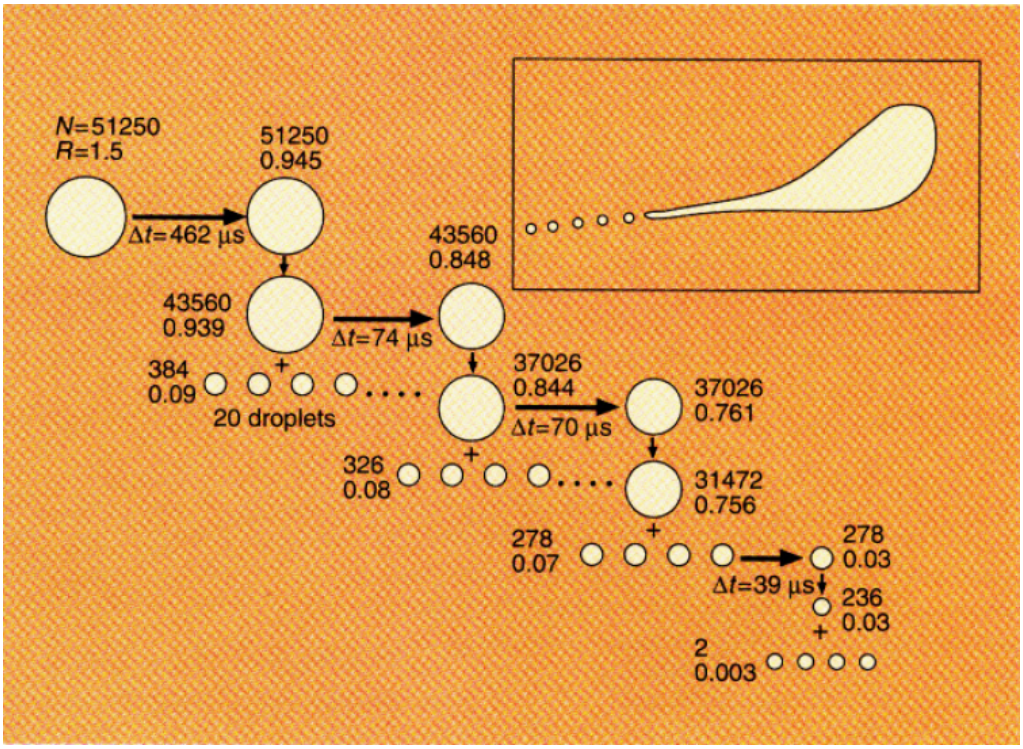

Figure 2.3: Schematic representation of the fission process of ESI droplets [22].

Limitations of ESI

ESI has many application and advantages, but the technique has some limitation that need to be considered. Some of these limitations are fundamental, others are yet to be overcome. In ESI the ions are formed by the accumulation of charge in the droplet. Thus one of the obvious factors that limits the output current is the electrochemical process that generates ions at the probe tip [3].

From the previous sections we can conclude that the number of ions created in the solution are only limited by the local concentration of the analyte. However the process of oxidation and reduction poses a secondary limitation, not caused by the flow but by the speed of the responsible processes to create ions and counter ions. In practice it is found that the maximum ion current is around 1 μA.

Besides the oxidation/reduction reactions and concentration of the analyte, the extraction of ions is also dependent on a complex combination of parameters such as size of the capillary, nature of the analyte, applied potential or the surface tension to just name a few. Most investigations in the advances of electrospray are currently focused at understanding an optimizing these parameters in ESI. The challenge lies in determining the parameters that are solvent independent and coming up with an accurate model to describe the underlying processes [3]. Because of the complexity of the underlying processes and the many parameters that it relies on, the search for improvement is a tedious and not straight-forward task.

Another limitation of ESI lies in the ability to ionize hydrophobic proteins in their natural environment. The next section will clarify the interest in these proteins. These types hydrophobic protein analytes can be studied with ESI by using different solvents than water. Intact membrane protein complexes are an example of these hydrophobic proteins. Recently it is successfully tested that these substances can in fact be transferred to the gas phase using ESI by encapsulating the substance in phase detergent micelles [23].

(clinical) Applications

To close the section about ESI we will discuss a few of the clinical application of the method. ESI has proved to be a very powerful technique in the identification of proteins [24, 25, 26]. The samples are normally in very (small) amount available which makes ESI one of the best research techniques in determining the structure. This process is called protein sequencing, one of the clinical applications of mass spectrometry. One of the main interests for proteins lies in finding mutated proteins. The mutated variants of proteins lead to differences in molecular weight. Theoretically the combination of ESI and a mass spectrometry (ESI-MS) could characterize most protein mutation, but for now the widely studied protein is haemoglobin [27]. It should be noted there are still some limitations to this technique when the mutated proteins only have a different sequence or the mutated amino acids have the same mass.

Besides the characterization of samples in (bio)-chemistry and medical researches, ESI-MS has found practical applications to diagnostic 'hard to spot' diseases. The most common clinical application lies in the screening of inborn errors of the metabolism [28]. Many of these deficiencies can lead to serious health issues among which mental retardation, physical handicaps or even death.

Doctors started using ESI-MS in the beginning of the '90, where it was used to diagnose patients and today state of the art computerized ESI-Mass spectrometers are able to significantly improve the screening time and processing of the results. Example are Neonatal screening for cholesteric hepatobiliary diseases, screening for disorders in metabolism and detecting earlier stages of diabetes [29]. Besides the applications in hospitals ESI-MS has also found an application in crime scene investigation where it is used to examine evidence in sexual assault investigations where the assailants use condoms to hide their genetic fingerprint. With ESI small amounts of analyte can be retrieved and analyzed [30]. These examples of applications are a result of advanced techniques which could only be developed due to the use of ESI in the first step of the process. It remains a highly speculative what advanced techniques could be derived from an improved ESI performance.

2.2 Quadrupole ion trap

In 1953 Wolfgang Paul published a paper describing the mathematical framework that described a new type of mass-spectrometer that makes use of a quasi-stationary electric field using an alternating potential [31]. A charged particle cannot be trapped in a static electric field and therefore a dynamic oscillating field is needed. This theory has later been used to construct a trap in which masses are not only kept in a stable motion at the center of the trap, but can be selected as well. The technique to trap and study particles was a revolutionary technological breakthrough at the time. In fact, in 1989 Wolfgang Paul shared the Nobel prize together with Hans Georg Dehmelt for developing the ion trapping technique [2].

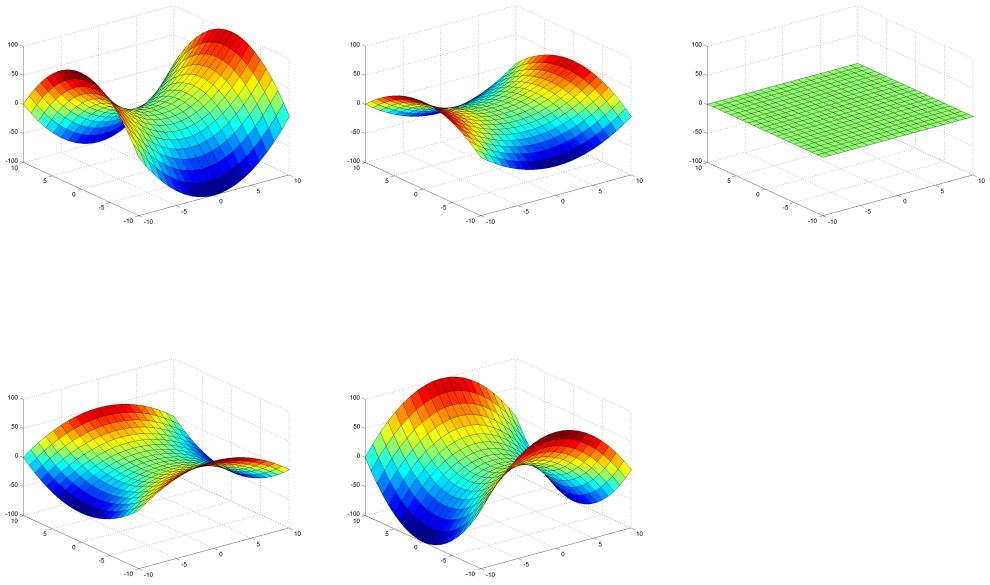

Figure 2.4: Five subsequent images of the oscillating potential inside the quadrupole trap (arbitrary units on the axes). The actual potential will make a continuous 'flapping' motion visualized by going from the top left image to the bottom right image and back.

The discovery of this technology in which you can observe small particles in free space without any other interactions springs from the questions what would happen with charged particles in multiple electric fields [2]. The

quadruple ion trap, also named 'Paul-trap' after one of its inventors is the nearest approximation to this stable levitation of particles. The trap consists of a hyperbolic shaped ring enclosed by two hyperbolic rotationally symmetric caps on the top and bottom of this ring. Nowadays quadrupole ion traps have many applications that extend to commercialized applications such as mass selectors in mass-spectrometers [1].

The working principle of the ion trap can be visualized with an 3D image of the static electric field within the trap. According to Earnshaw's theorem, a collection of point charges cannot be kept in stable stationary equilibrium by only using electrostatic interactions. Intuitively this is clear as well: a charged particle will always be attracted to the highest positive or negative potential. Figure 2.4 shows the 3D potential of the electric field inside the trap. We can make a mechanical analogy to explain how the particles get trapped. Imagine a 'ball', representing the droplet, at the center of the plot, shown in figure 2.5. The saddle shaped potential allows the ball to roll off on two sides. However when we spin this saddle around fast enough, fast enough so that the ball can't follow this motion, the ball will remain trapped at the center [2]. Although the analogy has some obvious discrepancies it remains a strong intuitive explanation for the underlying process.

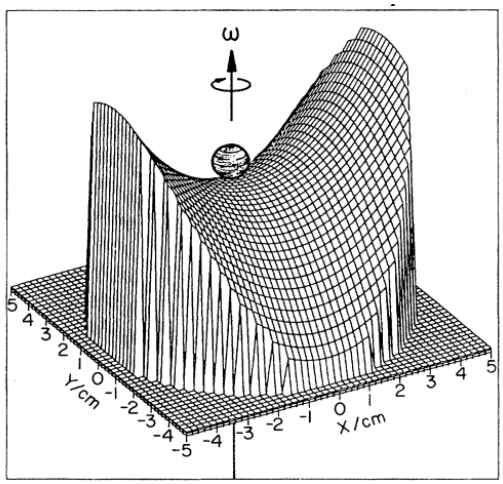

Figure 2.5: Mechanical analogue where the surface represents the potential and the ball in the center represents the particle. Copied from [2].

The 'spinning' in this analogy is obtained by a fast oscillating electric field inside the quadrupole trap. This electric field is constructed by applying an oscillating potential to the ring electrode or the end caps. If this oscillation potential is fast enough it will results in the trapping of charged particles. This charge particles exhibit a large and a micro oscillating motion around the center of the trap. Additionally an DC potential can be superimposed to compensate for gravity and guarantee confinement in the axial direction by increasing the potential dept at the center of the trap. The frequency of the oscillating potential is determined by the mass and charge of the particle.

2.2.1 Stability in the Quadrupole ion trap [2]

The relationship between force and electric potential energy is given by:

$$F = -Q\mathbf{E} = Q\nabla\Phi \tag{2.4}$$

Where Q is equal to the charge in the field and Φ represents the potential of the electric field. An ideal potential has the form of $\Phi = \frac{\Phi_0}{N}[A\hat{x}^2 + B\hat{y}^2 + C\hat{z}^2]$. In this equation N represents a normalization factor and A, B and C are constants.

This potential has to satisfy the Laplace's equation $\nabla^2\Phi = 0$. In this case we deal with rotational symmetry around the z-axis which leads to the fixed constants of A = B = 1 and C = -2. Because of this rotational symmetry we can shift toward a cylindrical coordinate system by replacing $\hat{x}^2 + \hat{y}^2 = \hat{r}^2$:

$$\Phi = \frac{\Phi_0}{N}[\hat{x}^2 + \hat{y}^2 - 2\hat{z}^2] = \frac{\Phi_0}{N}[\hat{r}^2 - 2\hat{z}^2] \tag{2.5}$$

As described in the introduction, the underlying principle of a quadrupole trap is based on applying a dynamic oscillating potential together with an optional static potential applied to the ring electrode. For the derivation we assume that both are nonzero. This will create a potential of the form:

$$\Phi = \frac{U_0 + V_0\cos(\Omega t)}{N}[\hat{r}^2 - 2\hat{z}^2] \tag{2.6}$$

We want to trap a particle inside the trap, which is possible due to the inhomogeneous nature of the oscillating potential. This field results in a force directed to the center of the trap. If the oscillating potential is fast enough so that the mass of the charged particle in the trap causes the particle to converge in space to the center of the trap.

Making use of Newton's second law ($F = ma$) and set it equal to the force acting on a charged particle in an electric field ($F = -Q\mathbf{E}$) for a charged particle with mass m_0 and charge Q:

$$F = m_0 * a = m_0\frac{d^2u}{dt^2} = -Q\frac{d\Phi}{du}, \qquad u = r, z \tag{2.7}$$

Which results in the equation of motion in the radial and z direction:

$$\frac{d^2r}{dt^2} = -\frac{2Q}{Nm_0}(U_0 + V_0\cos(\Omega t)r \tag{2.8}$$

$$\frac{d^2z}{dt^2} = \frac{4Q}{Nm_0}(U_0 + V_0\cos(\Omega t)z \tag{2.9}$$

Both these equations can be written in the form of the general Mathieu equations:

$$\frac{d^2u}{d\tau^2} + (a_u - 2q_u\cos(2\tau)) = 0 \tag{2.10}$$

In the case of the quadrupole trap we get the following a_u, q_u and τ parameters:

$$a_r = \frac{8QU_0}{Nm_0\Omega^2}, \qquad q_r = -\frac{4QV_0}{Nm_0\Omega^2}, \qquad \tau = \frac{\Omega t}{2} \tag{2.11}$$

$$a_z = -\frac{16QU_0}{Nm_0\Omega^2}, \qquad q_z = \frac{8QV_0}{Nm_0\Omega^2}, \qquad \tau = \frac{\Omega t}{2} \tag{2.12}$$

Solutions to the Mathieu differential equations are well studies and have exact theoretical solutions. With the aid of the Floquet theory one finds that the general solution of the differential equation is in the form of:

$$u(\Omega) = e^{\mu\Omega}\phi(\Omega) \tag{2.13}$$

where $\phi(\Omega)$ is a periodic function such that $\phi(\Omega + 2\pi) = \phi(\Omega)$. Because of this periodicity this can be expanded in a Fourier series of the form:

$$\phi(\Omega) = \sum_{n=-\infty}^{\infty} A_n e^{i2nt} \tag{2.14}$$

By making use of the last equation as a solution for equation 2.10 one can find an expression for the stable solutions of this differential equation. These expressions make use of the symmetry and antisymmetry of the Fourier series which lead to four classes of solutions that can be numerically solved. The full derivation of this is a common subject for most advanced math courses and can be found in most (advanced) calculus books. As a solutions we get an q_u versus a_u plot where the solutions for boundaries of stable and unstable regions . In figures 2.6a and 2.6b we can observe such a plot in which we have shaded the stability regions for both the radial and axial direction. The plot for the z-direction is made by making use of the relations between the two directions as derived from equations 2.11 and 2.6b from which it can be derived that $a_z = -2a_r$ and $q_z = 2q_r$ where the last equation loses it's minus sign due to symmetry of q_u around the a_u axis.

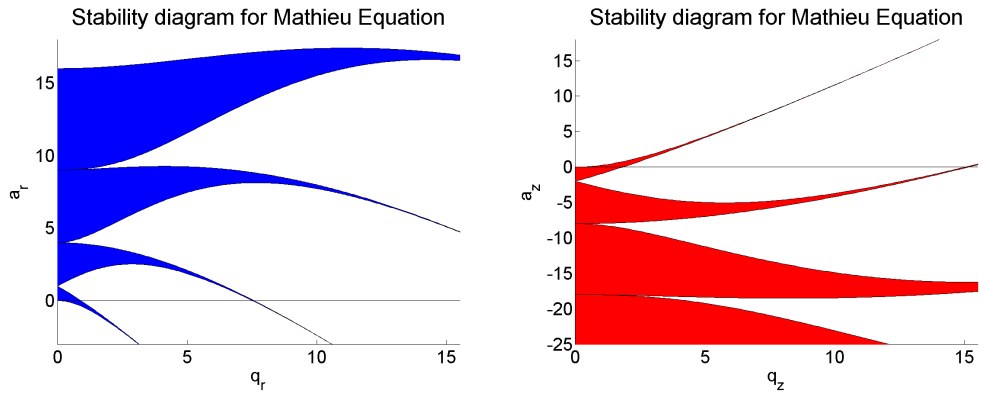

(a) Solution in the a_r versus q_r direction **(b)** Solution in the a_z versus q_z direction

Figure 2.6: The first set of solutions to the Mathieu equation. The shaded regions represent the stable solutions in the radial- and the z-direction

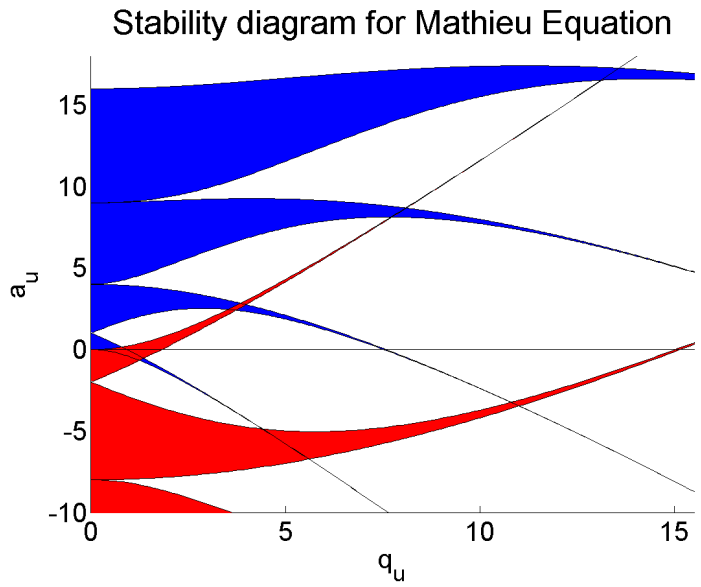

Figure 2.7: Overlap of the stable regions of the radial- and z-direction solutions to the Mathieu equation.

If we combine both these plots we end up with figure 2.7. We can see there are two areas where both stability regions overlap. For now we will focus on first stability region close to the origin of the axis because there we can simplify the analysis by setting the static potential, U to zero. A close up of this first

stability region is shown in figure 2.8. From this numerical computation we can extract the boundary values for which we still have stable solutions in the quadrupole trap.

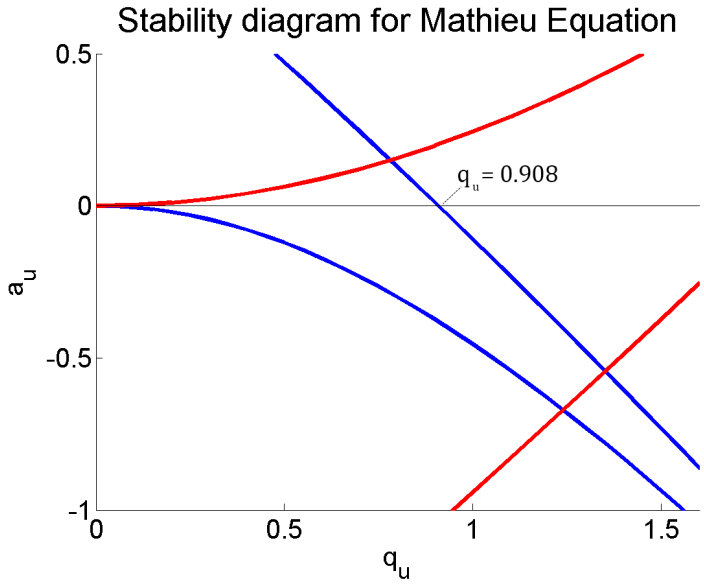

Figure 2.8: Close-up of the first stability region overlap for radial and axial direction. This numerical solution states the stability parameters for the quadrupole trap. If we set static potential, U to zero we can find the maximum stability parameter on the x-axis to be $q_u = 0.908$.

2.3 Fluorescence

With the experimental setup we want to study the internal molecular distribution of microdroplets inside a quadrupole. In particular we want to study the distribution as a function of time, which due to evaporation of the droplet represents a stage in the disintegration of the droplet. To study the molecular distribution we make use of a technique based on fluorescence microscopy.

We will image the droplets with a camera, making 2D images of the droplet. To understand what we are seeing with the camera we have to explore the working principle behind fluorescence and how to use the techniques of fluorescence microscopy in this setup. Sir John .F.W. Herschel was the first to observe and describe the process of fluorescence in 1845 [32]. In his report he writes about the observation of a "beautiful celestial blue color" emitted from a quinine solution in sunlight.

Fluorescence is the process where a photon is absorbed by a atomic or molecular system, and then after a certain time a photon is emitted from this system. As a prerequisite, to be absorbed by the system, the photon has to contain enough energy to overcome the gap between the ground state and a higher electronic level This process is called stimulated absorption because the incident photon stimulates the system to absorb a photon.

Subsequently the excited state relaxes to the lowest available vibrational energy state either by vibrational relaxation or by internal conversion (excited electrons that transition from strongly overlapping electronic energy level). After the so called fluorescence lifetime the electron in the exited state returns to the ground state and emits a photon, which is called spontaneous emission. Energy is lost due to non radiative processes such as vibrational relaxation or internal conversion and therefore this photon has a different energy than the initial photon. A photon with a different energy and thus a different wavelength is emitted from the molecular system.

Fluorescence is usually illustrated with a Jablonski diagram such a shown in figure 2.9. In this Jablonski diagram the first three electronic states are drawn: the ground state S_0, the first and second electronic state S_1 and S_2 respectively. Above each state the vibrational states are indicated. An incoming photon excites the system to one of the exited states. This has a typical transition time of 10^{-15}s (fs). Subsequently the higher vibrational states relax to the lowest exited state. This process of vibrational relaxation or internal conversion typically takes 10^{-12}s (ps). Then due to thermodynamic equilibrium the electron in a higher state relaxes to the ground state while emitting the fluorescence photon. The time an electron stays in the exited stated is defined as the fluorescence lifetime, and is typically in the order of 10^{-8}s (10ns) [33].

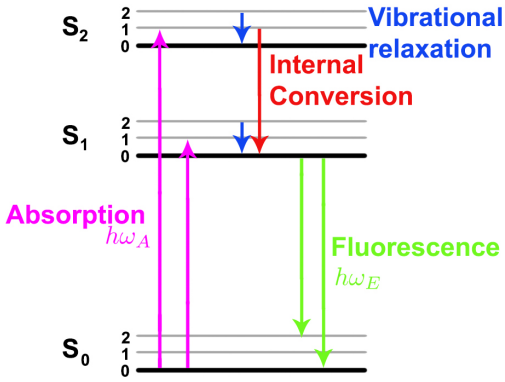

Figure 2.9: Schematic Jablonski diagram with energy and vibrational levels. Adapted from [33].

Einstein was the first to describe the processes of spontaneous emission and induced absorption in terms of probabilities. These probabilities define the

lifetime of the photons in an excited state and are named after it's inventor as the Einstein stimulated absorption/emission (B) and spontaneous emission(A) coefficients. The emission coefficient A is defined as the total rate of spontaneous emission from a higer to a lower level, eg. 2 to 1 (W_{21}^s) for a system of N_{exited} atoms in the upper level:

$$W_{21}^s = A_{21} N_{exited} \tag{2.15}$$

If this excited level can only decay by this radiative relaxation the spontaneous lifetime of that state is defined by:

$$t_{spontaneous} = \frac{1}{A_{21}} \tag{2.16}$$

Similarly the stimulated absorption coefficient B is defined as the transmission rate as a function of the energy incident to the system. Here the ρ_ω represents the energy density per unit angular frequency interval in the region of the ground and exited levels of the atom [34].

$$W_{12}^i = B_{12}^\omega \rho_\omega N_{ground} \tag{2.17}$$

To reach a stream of continuous fluorescent photons, electrons have to be continuously promoted from the ground state to the excited state. This is achieved by stimulated absorption through a laser with a specific constant wavelength that matches the band gap between the ground level and an exited level. When an equilibrium is reached and a continuous stream of photons is absorbed and emitted.

The droplet dynamics we want to study have a lifetime in the microsecond range. The process of fluorescence has a combined lifetime in the order of 10ns which make it very suitable as a method to study a droplet inside the quadrupole trap.

Each molecule that can undergo fluorescence has a characteristic absorption and emission spectra, as an example the spectrum of the molecule NBD-CL is shown in figure 2.10. In a later section we will determine that NBD-CL is a likely choice to use in this experiment.

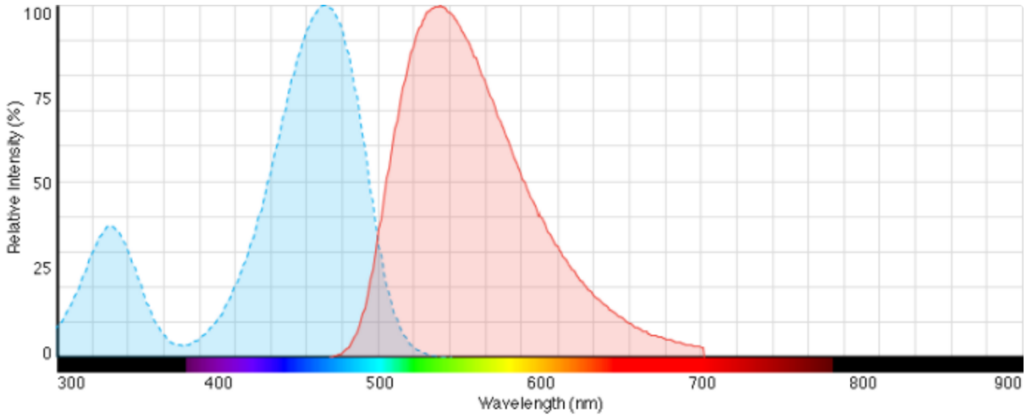

Figure 2.10: The absorption and emission spectrum of NBD-CL. The blue graph represents the absorption spectrum for which the molecule is transfered to the excited state. The red curve represents the emission spectrum. If the electron is promoted to the same levels as from which it decays, then the difference between the absorption and emission peak is defined as the Stokes shift [33, 35].

2.4 Abel Transform

The experimental setup will be discussed in the next chapter, however in this section an technique is described that is related to the setup. Figure 2.11 shows a schematic overview of the setup. The droplet is radiated by a diode laser and the resulting fluorescent photons are imaged by an CCD-camera perpendicular to the laser beam. The image of the droplet is a 2D projection of the 3D droplet. We want to study the distribution of molecules inside the droplet which means we have to relate the 2D intensities that can be extracted from the images to an three dimensional droplet image.

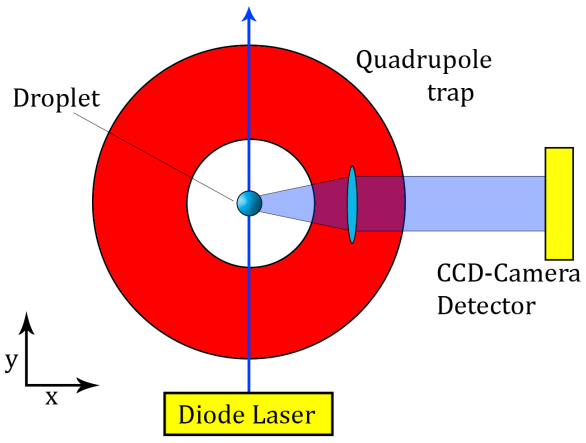

Figure 2.11: Schematic top view of the setup with the quadrupole trap at the center.

Figure 2.12 shows a schematic cross section of the droplet that we want to image perpendicular to the laser beam. If we assume that the droplet has a spherical symmetry in the z-direction we can make use of the continuous parallel-projection abel transform [36]. This can be generalized to include the z-direction of the spherical symmetric object which has as the result:[37]:

$$P(x,z) = 2\int_{|x|}^{\infty} \frac{rI(r,z)}{\sqrt{r^2-x^2}}dr \tag{2.18}$$

Where $P(x,z)$ represents the 2D projection of the 3D image $I(r,z)$.Because the camera captures a projection of the droplet we want to use the inverse form of this Abel transformation[38] which is given by:

$$I(r,z) = -\frac{1}{\pi r}\int_{r}^{\infty} \frac{[dP(x,z)/dx]}{\sqrt{x^2-r^2}}dx \tag{2.19}$$

This inverse Abel transform is the product of a mathematical derivation and has been proven to be impractical with numerical analysis because the formula contains singularities and it is needed to estimate the derivative of generally noisy data [37]. There have been numerous attempts to solve the inverse Abel transform by either fitting the numerical data to acquire an accurate derivative [39], using additional transformations of the Abel transform [40] or by expanding the projection in a basis set of functions [37].

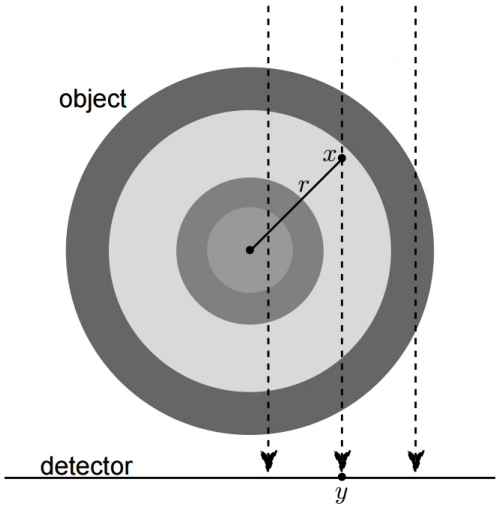

Figure 2.12: Schematic top view of a cylindrical symmetric object imaged by detector. Figure adapted from [36]

An way to overcome the problem of inverse Abel transform is to model the input intensity function and calculate the Abel transform according to formula 2.18. There are several distributions to consider: fluorescence intensity at the center, the boundaries and somewhere in the middle of the droplet. By simulating different intensity distribution with linear function we can solve the integral of formula 2.18 exact by making use of standard

integrals. Three different distributions have been transformed and the results are shown in figure 2.13. By analyzing measured data and going though an iterative process of changing the input intensity distribution it is possible to come up with a model that fist closely to the measure data. This way the exact inverse Abel transform is unnecessary to consider. Which of the two techniques will be used is dependent on the quality of the data.

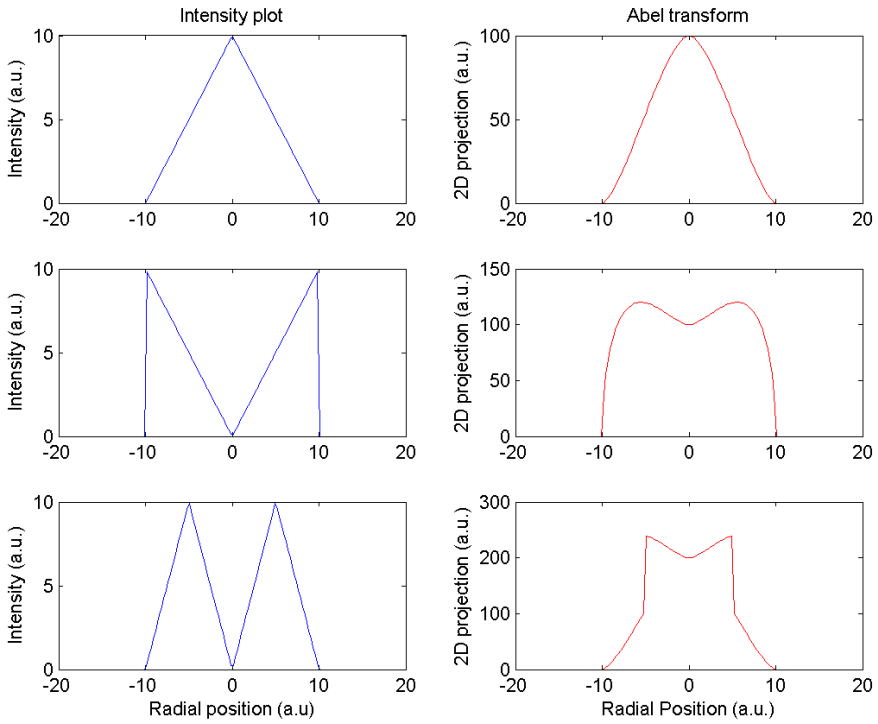

Figure 2.13: Radial intensity distribution and the Abel transformations that result from these distributions. The left column represents the intensity distribution and the right column represents the Abel transformed intensity. The top two plots represent an linear increasing distribution where the peak intensity lies at the center of the droplet. The resulting transformation has a trivial shape. The second row represents a distribution where the intensity lies at surface of the droplets and generates an Abel transformed intensity pattern that is not intuitively clear. The bottom row show a distribution where the intensity is placed at an intermediate position.

2.5 Evaporation models

The electrospray ionization section ends with the notion that the ionized analyte is transferred to the gas phase. Since the discovery of ESI, analytical chemists are working on the development of a complete model that describes this transition. Coming up with an accurate model turned out to be a surprisingly difficult task [41, 42]. With the aid of molecular dynamics simulations, new insights in the process of evaporation have been developed. At the moment there are two widely accepted models that respectively describe the evaporation of low and high molecular weights analytes. These are referred to by the 'ion evaporation model' (IEM) and the 'charged residue model' (CRM) respectively. In addition to these two models an chain ejection model (CEM) has been proposed for unfolded polymers [7].

IEM: The initial drop has gone through several fission steps and we are left with a nanometer sized droplet that has a radius below 10 nm. The electric field inside the droplet that is a result the size and charge of the droplet is capable of ejecting clusters of ions from the droplet. Aided with molecular dynamics simulations it is found that when the ion is departing the droplet it remains connected through a 'sticky' string of solvent molecules [43]. The connection then ruptures and we are left with a small gas-phase cluster consisting of an ion and some solvent molecules.

CRM: For larger molecular weight species it is believed that the fission of the initial droplet results in a nano-droplet that contains only a single analyte molecule together with solvent molecules. As the solvent molecules evaporate, the charge is further transferred to the analyte [22, 44]. It is found and confirmed by molecular dynamics simulation studies that the droplet remains close to the Rayleigh limit and can emit charge by IEM ejection. Finally the single analyte is evaporated to dryness and we end up with an ionized gas-phase molecule.

CEM: Most large biomolecules such as proteins have a folded structure which remains folded throughout the solution. When the molecule has a hydrophobic core that is not accessible by the solvent [45] the evaporation model follows the above described CRM. Molecular dynamics simulations have shown that unfolded proteins behave differently and do not follow IEM or CRM. This unfolded protein switches its properties from compact-hydrophobic to extended-hydrophobic with as result that the hydrophobic parts of the molecule will migrate to the surface of the droplet. This chain then can be transferred to the gas-phase by step-wise ejection from the droplet.

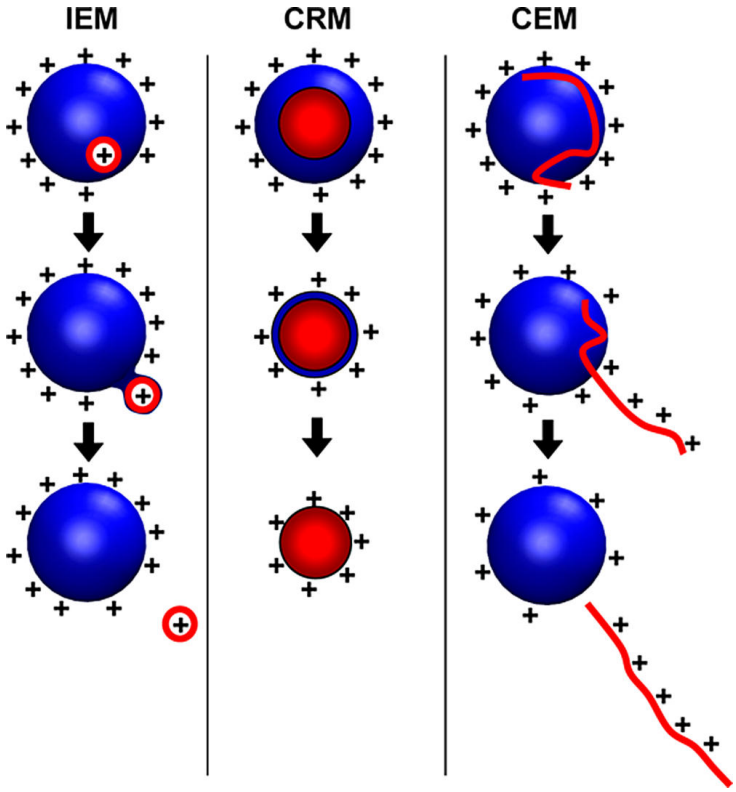

Figure 2.14: Summary of the three different models used to describe the ESI mechanism. IEM: small charge ejection from the droplet. CRM: evaporation of the solution around the analyte. CEM: ejection of an unfolded protein. Red and blue represent the analyte and solvent respectively. Figure copied from [7]

The three processes have been schematically shown in figure 2.14. The described models have been proven to be useful for their respective boundary conditions, however it still remains an active field of research to combine the characteristics of the models to end up with one model that is able to describe intermediate states [7].

Chapter 3

Experimental setup

"No amount of experimentation can ever prove me right; a single experiment can prove me wrong."

— Albert Einstein

The experimental setup is based on a similar experiment performed by a joined research team consisting of the Centre Interdisciplinaire de Recherche Ions Lasers (CIRIL) and the Insitut für Physik, Technische Universität Ilmenau in Germany. They studied the behavior of droplets when they reaches the Coulomb instability [46].

Already in the introduction it is described that Leisner et al. were able to capture the process of disintegration of microdroplets by using a very intense flashlight and a variable delay. The experiment described in this section is focused on collection of data to understand this instable disintegration process more accurately. Leisner et al. showed that their models are able to predict part of the deformation process of critically charged microdroplets [9]. This experiment will overcome their limitation of considering the droplet as a whole by tracking the molecular distribution of the analyte inside the droplets.

3.1 Quadrupole ion trap

Section 2.2 describe the trapping of ions inside a quadrupole trap and together with the mathematical foundation described in that section we can understand how charged levitate droplets are generated inside the trap. In

this setup we use a trap that has been obtained from an obsolete mass spectrometer and a schematic model of the trap is shown in 3.2. The two hyperboloidal shaped top and bottom electrodes are placed at approximately 7.4 mm from the center of the trap. The hyperboloidal torus electrode, encapsulated with an an insulating from the top and bottom cap has an internal radius of 10mm.

A pulse/delay generator, 555 series developed by BNC in the USA is used to trigger the droplet dispenser and a camera. A home-build synthesizer box generate a sinusoidal signal of which the amplitude and frequency can be tuned. This signal is amplified by an 2HVA24-BP1 high voltage Amplifier developed by Ultravolt in the USA that can provide an sinusoidal potential with an maximum amplitude of 2 kV depending on the height of the input signal. The upper stable frequency that this amplifier can handle is approximately 7 kHz. This potential is applied to the ring electrode of the quadrupole trap. The end cap electrodes can be connected to the ground or to an constant bias to increase the potential dept at the center of the trap.

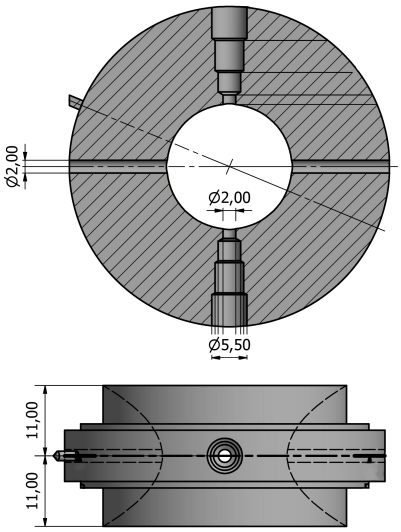

Figure 3.1: Top: Cross sectional view of the holes in the central torus of the quadrupole trap. Bottom: Side view of the torus.

In this setup we have only imposed an varying electric field on the ring electrode without an additional static electric potential because we assumed that the process of evaporation in much faster than the gravitation influence to withdraw the droplet from the trap. This assumption is based on private correspondence with the French group [9].

To use the quadrupole trap in this experimental setup it had to be adapted to fulfill its purpose. Two holes have been drilled through the exterior of the ring passing through the center. One hole has a diameter of 2 mm and is used to direct a laser beam on the center of the trap. Perpendicular to this hole, an expanding hole has been made to monitor the droplets with a camera. A cross sectional and side view of the trap is shown in figure 3.1.

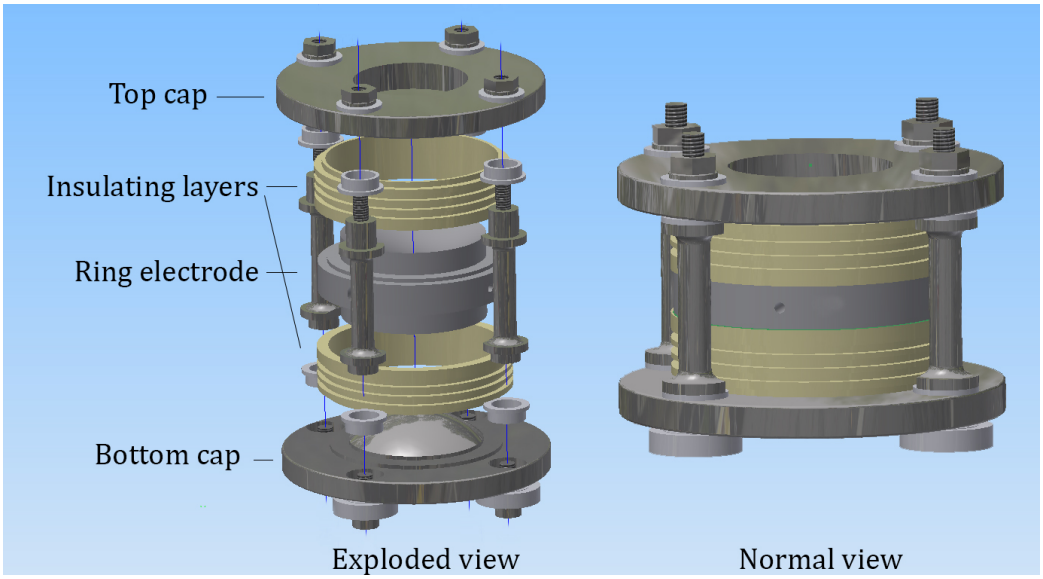

Figure 3.2: Drawing of the quadrupole ion trap used in the experimental setup (Truthful drawing made in Autodesk Inventor).

3.2 Charged droplet generator

A droplet generator (Micro-dispensing System MD-E-3000, Microdrop technologies, Germany) is used to generate droplets above the trap. The nozzle of this droplet generator consists of a glass capillary surrounded by a piëzo actuator. Due to this piëzo actuator, the micro dispensing system is able to generate droplet that range from 20 pl to 380 pl which corresponds to droplets with a diameter between 20 and 100 μm. The droplet generator can reproduce droplets up to a repetition frequency of 1450 Hz with an volume variation $<1\%$ [47]. A sequence of images in figure 3.3 shows a droplet emerging from the dispenser head.

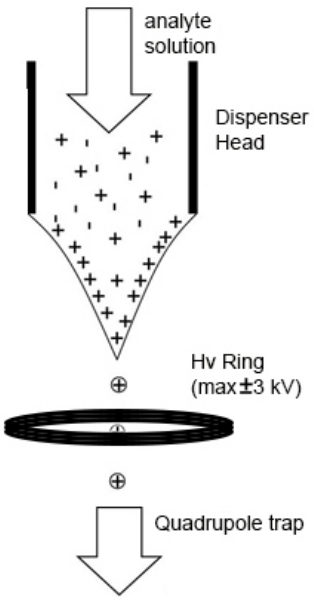

A technique very similar to ESI is used to extract charged droplets. In ESI the charged droplets are extracted by applying

a potential between the needle from which the droplets are sprayed and the mass spectrometer as shown in figure 2.2. In this setup we place a small conducting ring under the droplet dispenser nozzle in the opening above the top cap of the quadrupole trap. By applying a bias to the ring and placing the droplet generator directly above the ring without touching it. A bias up to ±3 kV can be applied to the ring which causes a potential difference between the droplet dispenser and the ring, ensuring the extraction of charged droplets. An schematic overview is shown in figure above.

The actual volume of the droplets generated by the dispenser head depends on the type of liquid and the surroundings in which the droplet generator is used. Therefore to determine the size and volume of the droplet there needs to be done a calibration. The most straight forward calibration method to determine the size of the droplets is by having an object with known size in the same image as the droplet and compare the sizes. Because of the high reproducibility of the droplet generator this only has to be done once for every parameter-solution configuration.

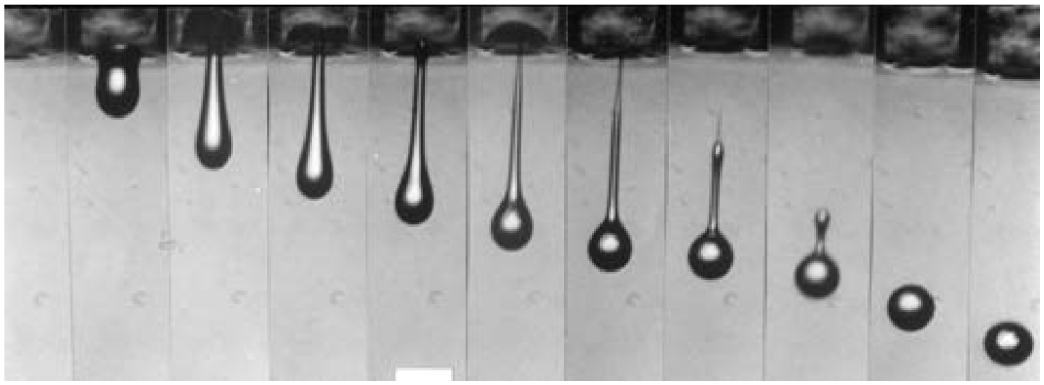

Figure 3.3: Droplets ejected from the nozzle of the microdroplet dispenser. The dispenser is capable to produce droplets at a frequency up to 1450 Hz with very little volume variation. (Picture copied from [48])

3.3 Camera & Laser

The camera used in the experiment is an old PCO Sensicam, manufactured by SD vision in Belgium that has been declared obsolete by the manufacturer, but still can fulfill the needs for this experiment. It can be externally triggered to capture an image, the exposure can be set between 0.1 and 1000 μs, the resolution is 480 x 640 pixels and the quantum efficiency of the sensors making up the pixels is >40% at 540nm [49]. The camera is still supported by the newest version of the software which allows the most advanced image handling and enhancement made possible my the manufacturer. On the camera a lens is mounted that can magnify the droplet up to 25 times.

We use an CPS450 (Thorlabs, Germany) blue (450 nm) diode laser to probe the droplets inside the trap. The choice of laser wavelength has been based on the fluorescent wavelength of NBD-Cl which has its fluorescence absorption wavelength centered around 480 nm as described in section 2.3 and shown in figure 2.10.

3.4 Experimental setup

Inspired by the experimental setup of the E. Giglio et al. [9] we have designed an experimental setup that can capture the molecular structure of microdroplets. An schematic overview of the setup as a whole is shown in figure 3.4b. The quadrapole ion trap operates at ambient pressure. An external trigger first sends a signal to the droplet dispensing system. Then, a second signal with a variable delay is send to the CCD-camera detector to image the droplet inside the trap. By assuming that the droplet is kept at the center of the quadrupole ion trap during the evaporation process, it is possible to capture the droplet at different stages of the evaporation process.

In combination with the fluorescent marker described in section 2.3, the molecular distribution of the analyte is represented by the intensity distribution of photons captured by the CCD-camera. As a fluorescent marker we will use NBD-Cl (4-Chloro-7-nitrobenzofurazan). This molecule has an excitation wavelength of 480 nm and a emission wavelength of 540 nm. By placing a filter between the droplet and the camera that only lets through photons with a wavelength above 450 nm, it is possible to image the position of the fluorescent markers. The resulting image is a 2D projection of the fluorescent molecules inside the droplet which can be transformed to a 3D distribution by making use of an Abel-transform as described in section 2.4.

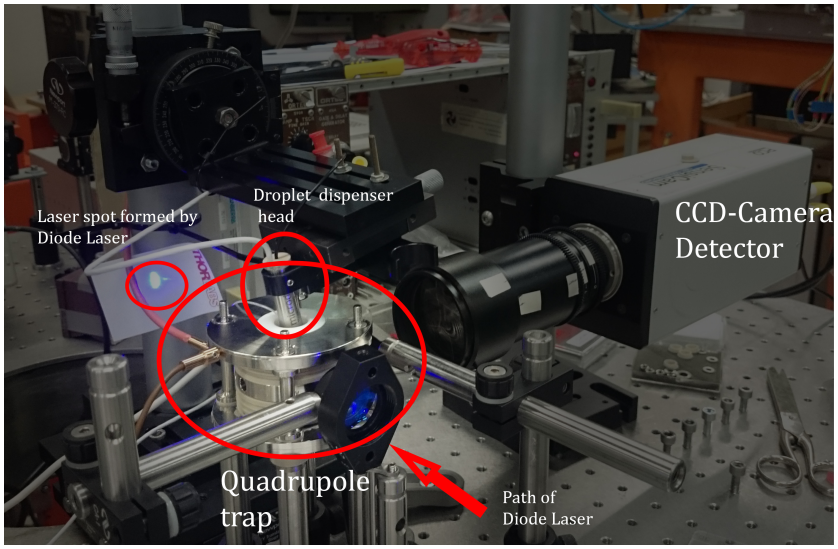

(a)

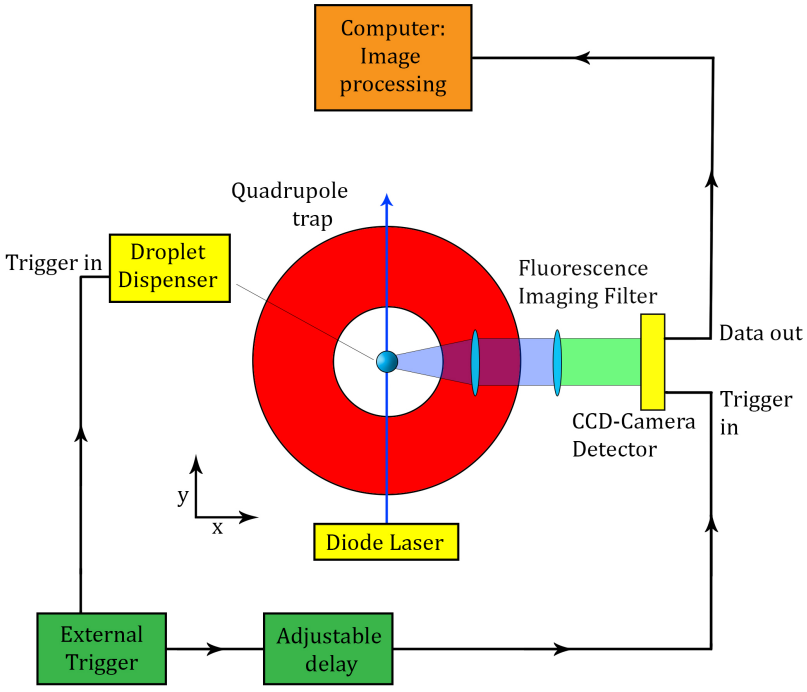

(b)

Figure 3.4: (a) Picture of the real experimental setup in the laboratory. (b) Schematic experimental setup (cross section through the horizontal plane of the quadrupole ion trap)

Chapter 4

Results and discussion

4.1 Results

The experimental setup described in the previous chapter has been build and used to test several parameter configuration which are described in this chapter. However before proceeding to the results section it should be noted that the experimental setup as described in the previous chapter is the results of testing several configurations, ending up with the one described. During testing, the whole systems has been mounted on perpendicular glider rails where the position of the camera and laser as a function of the distance from the quadrupole trap could be adjusted. However it proved to be rather difficult to align the three systems. Practice has shown that it is easier to place and align the three systems independently.

In addition to the mounting of individual components it has been seen that the setup is prone to vibrations. Vibrations of the table and the mounting system of the setup were clearly visible in the images taken from the droplets. Therefore extra attention has been devoted to stabilize the individual elements of the setup.

4.1.1 Droplet dispenser

The manual of the droplet dispenser claims to produce droplets that have very little volume deviation, even at a high repetition rate. We have checked this in the setup of the laboratory. The microdroplet dispenser includes a camera that can be used to image the droplet directly under the dispenser head. In figure 4.1 we can see a droplet at different delay times after the trigger. This droplets sequence is made by changing the delay between the

dispenser head trigger and the capturing of the camera. In the sequence we see, each picture is a different droplet. It is clear from this that the apparatus is able to produce very similar droplets at the repetition rate as high as 1450 Hz.

When making close up images of the droplets we saw that the droplets do not fall straight down from the dispenser head. This skewed path is clearly visible in figure 4.2. The droplets are emitted at an angle of approximately 45 degree with respect to the plane of the image. From figure 4.1 it can also been seen that this skew is not only in the plane of capturing, but the focus of each picture is adjusted before capturing. In the first image the dispenser head is clearly visible, while is completely blurred out in the last image.

The conclusion that can been drawn from these images is that the dispenser head is capable of producing very similar droplets at a high repetition rate. This is needed for the experiment to work: droplets that are reproducible in time and space. However the angle between the dispenser head and the droplet is not desirable for the experiment, it would be more convenient if the droplets fall straight down. It is possible that in our case this skewed path it is caused by (permanent) contamination of the dispenser head. At one point during the testing of the dispenser head we saw a double streams of droplets emerging from the dispenser head, each stream leaving the dispenser head under a different angle in a different direction.

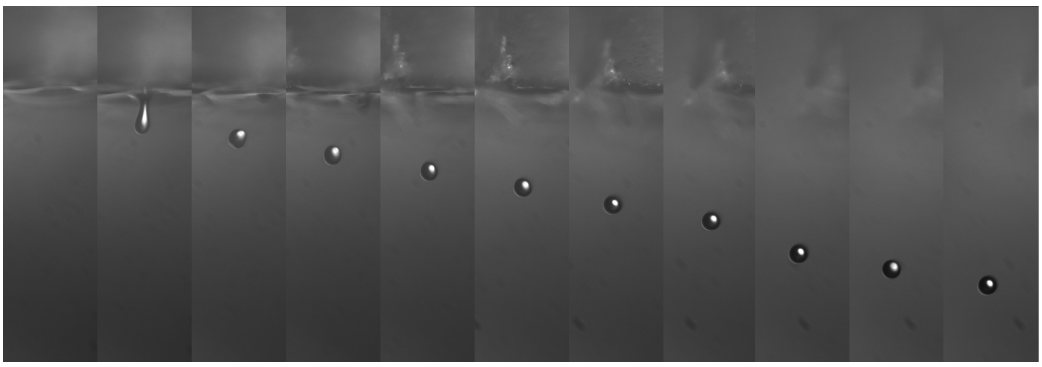

Figure 4.1: Sequence of droplets captured in the laboratory. Droplet is air have a typical falling speed of 2-3 m/s [47]. Images are taken from this experimental setup using the camera provided by the Microdroplet system.

Figure 4.2: Closeup of the same sequence of droplets as in figure 4.1 placed in a single figure without spatial rearrangement. It can be clearly seen that the droplet follow a skewed path with respect to the dispenser head.

4.1.2 Grain of sand

To confirm the working of the quadrupole trap in this experimental setup it was proposed to trap a grain of sand. A grain of sand has the advantage that it does not evaporate and thus will remain floating at the center of the trap. The sand for this test was acquired from a sandblasting device, which uses very fine and uncontaminated grains of sand. Unfortunately the size of these grains of sand are not constant and therefore could not be used to calibrate and determine the size of objects in pictures taken by the camera.

To trap the grains with a potential within the trap, the grains have to be charged. For this experiment it has been done by using a regular plastic ruler and charging the ruler by rubbing it over a suitable cloth. The ruler accumulates static charge which can be used to attract charged grains of sand from the sand reservoir. By gently tapping onto the ruler these grains of sand could be deposited in the trap.

The grains of sand lost their charge when they hit the top cap of the trap which was set at ground potential. To overcome this contact a miniature funnel was used to guide the grains through the tiny opening of the top cap.

It was a hard an tedious task to transfer a grain of sand with charge to the center of quadrupole trap without the grains accumulating to much speed to be caught within the potential of trap. By persistently trying to deposit the grains an grain was eventually captured in the trap. The grain showed a periodic movement predicted by the quadrapole theory and while the grain was inside the trap, changing the parameters linked to the potential caused a direct effect onto the movement of the grain. By adjusting the frequency and observing the motion of the grain of sand, a frequency range in which the grain was still trapped is determined. A sequence of images of the grain is shown in figure 4.3.

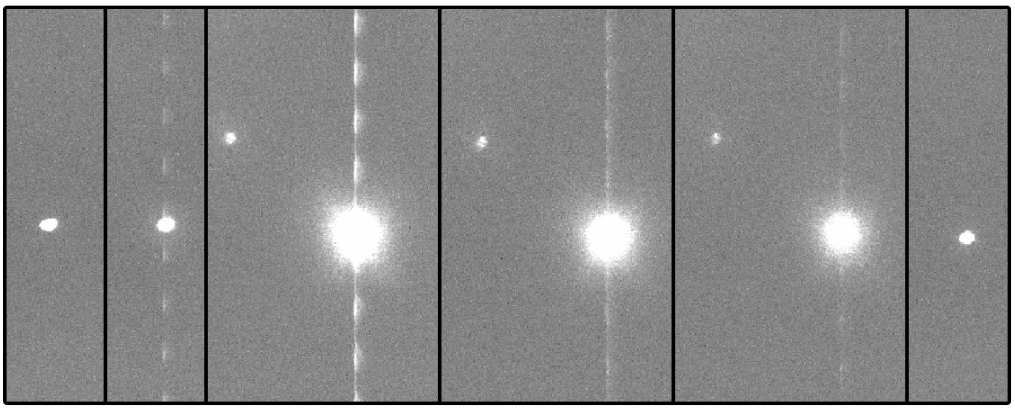

Figure 4.3: A sequence of a trapped grain op sand. The frames around each picture are not the same size because some frames show a secondary reflection. This secondary reflection could originate from several sources: a secondary grain, double reflection of the grain or the misalignment of the lensing system. Setup parameters: Exposure = 100μs, Quadrupole ring voltage = $\pm$ 1500V @ frequency range = 238 Hz - 539 Hz

Several conclusions are drawn from this result. First: the quadrupole trap works, charged particles can be trapped. Secondly: what we see on the images is laser light that is reflected by the particle inside the trap where the periodic movement of the particle causes the intensity of reflection to change in time. The intensity of reflected light is dependent on the relative position of the particle to the laser beam. For the droplet we need to stabilize the

particle and adjust the camera settings to get a clear image. All images in 4.3 are overexposed.

Last conclusion is that we see reflections in the form of a dashed line and a secondary particle. These reflection became a recurring observation in the further experiments with the actual droplets. The reflections are clearly visible in figure 4.4, where we not only see a secondary reflection, but also see an interference pattern of the reflected light.

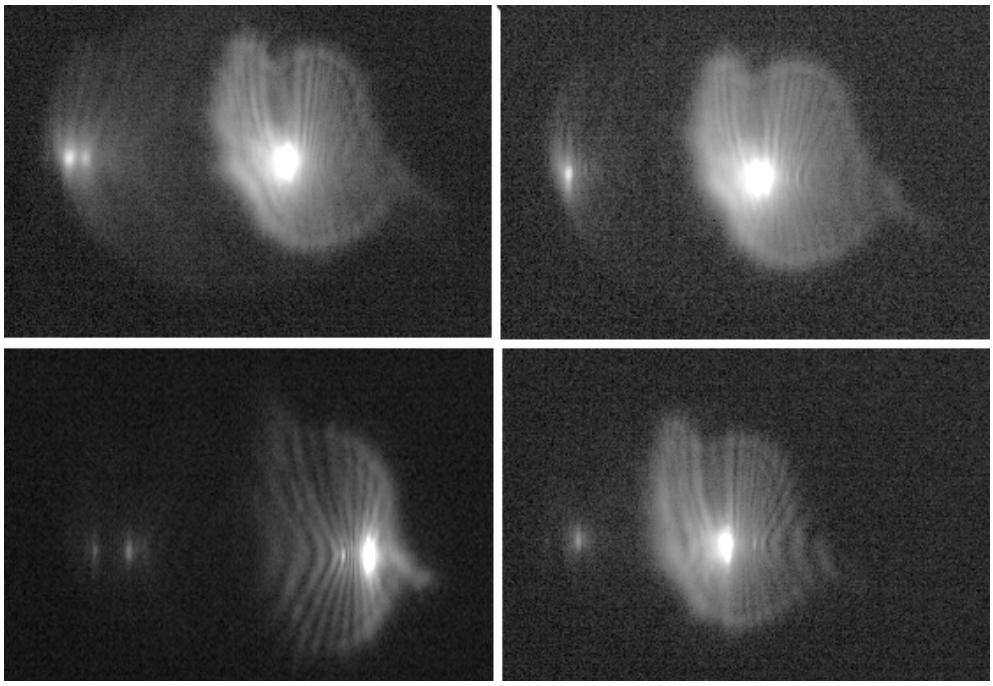

Figure 4.4: A series of images taken to illustrate the reflection. A droplet is deposited from a solution of pure H_20 with an arbitrary amount of NaCl.

Initially it was tough that the reflections were caused by the inner surface of the trap itself. To minimize the reflections and interference we coated the inside of the trap with colloidal graphite. This is a paint that masks the reflective properties, but maintains the electric properties. Maintaining the electric properties is necessary for the working principle of the trap. After coating the inside of the trap we still saw the reflections from the droplets. This indicates that the reflections and interference is caused by the (mis)alignment of the lensing system.

4.1.3 Droplets of water and NaCl

The next step is to capture droplets spawning from the droplet dispenser inside the trap. If this can be successfully reproduced, fluorescent molecules could be added to the fluid and the molecular distribution of these molecules can be studied.

Figure 4.4 in the previous section displays droplet captured on the inside of the trap. These droplets passed entered the quadrapole trap but are not stability caught at the center. To determine the trapping parameters that do trap droplets we performed a sweep in which we gradually changed the trapping parameters. The different parameters that have been swept are:

1. The frequency with which the dispenser deposits droplets.
We want to know what the delay is between the droplet and its arrival at the center of the trap. By adjusting the delay between dispensing and a pulse that triggers the camera we should be able to image single droplets. By starting at a high deposition frequency and gradually lowering the frequency while still maintaining the droplets in sight of the camera we were able to adjust the droplet deposition frequency down to 1 Hz.

2. The voltage of the ring electrode through which the droplets fall.
This parameters should influence how much charge is present inside the droplets. A higher charge would mean that the droplets are more affected by the oscillating potential. From this it is easy to conclude that the voltage applied to the ring electrode should be as high as possible. This voltage is limited by an electric discharge between the ring electrode and the cap or the droplet dispenser.

The distance a spark can travel in dry air is approximately 1mm per 1000V. The voltage of the ring electrode has been as high as ± 6 kV before a spark passed from the ring to a surrounding device. Because it is highly undesirable that sparks flow through the apparatus of the experiment, the high voltage of the ring is not raised above ± 3 kV during the sweeping of the other parameters. This upper limit is determined by comparing the magnitude to similar experiments [9] while keeping the safety aspect in mind.

3. The position of the droplet dispenser.
Because we had to deal with a stream of droplets that emerged from the dispenser head under and angle, we varied both the angle and the position of the nozzle with respect to the center of the trap. If the distance between the two is too high, the droplet already evaporates during deposition and never reach the center of the trap. If the nozzle is placed to low, the droplets are less influenced by the voltage on the ring electrode. Furthermore, the distance between the dispenser head and the ring electrode should not be so small that sparks can jump between them and possible damaging the dispenser head.

The direction and angle of the stream of droplets varied for each new instance and had to be aligned for every experiment. Secondly we had to prevent clogging of the input hole of the trap through which the droplets have to pass to reach the center. A higher depositing frequency cause this hole to clog. To clean this hole, the dispenser head had to be removed to access and the top cap input hole. After cleaning the hole the process of alignment had to be repeated which is a tedious and time consuming task and therefore most experiments were done at a relatively low droplet dispenser frequency ($<$500 Hz). It is concluded that automating this task of alignment could improve the reproducibility of the experiment. By having a stream of droplets falling straight down, this alignment could be eliminated entirely.

4. Frequency and voltage of the quadrupole ring electrode
Finally the frequency and voltage on the ring electrode of the quadrupole trap has been swept up to the limits of their range. The amplifiers maximum frequency is 7 kHz. The maximum voltage is $\pm$ 2 kV. Within these ranges both parameters have been swept by incrementing in small steps while a continuous stream of droplets was deposited inside the center of the trap. This sweeping was done manually and by looking at the droplets imaged by the camera it could be determined if droplets were trapped at the center of the trap. From this it was clear that changing these parameters did have an effect on the droplets. We could see the droplets being affected by the potential of the ring because of the induced movement cause by the change in voltage and frequency. However we did not trap an droplet in the center. By gradually changing the delay between imaging we could see the droplets pass from the top of the imaging to the bottom, effectively flying through the trap without being trapped.

Conclusion

We were not able to trap a droplet in the center of the quadrupole trap by gradually changing the trapping parameters. By adjusting these parameters we were able to see the droplets fly by on the screen and being influenced by the electric field inside the trap. The next step after catching and maintaining a droplet at the center of the trap is to optimize the imaging parameters by fine tuning the lensing system so that we have clear image of the droplet, and by adjusting the exposure of the camera to capture the droplet without overexposure.

After having captured a sharp image of the droplet in the trap, we should calibrate the size of the image frame to determine the sizes of droplets. This can be done by inserting an object with a known size into the image frame. The size of this object should be very well known and ideally would be a tiny round ball that can be charged and inserted to the center of the trap. Because this ball would then be drawn to the exact same position as the charged droplets, we know that the determination of size at that position is correct.

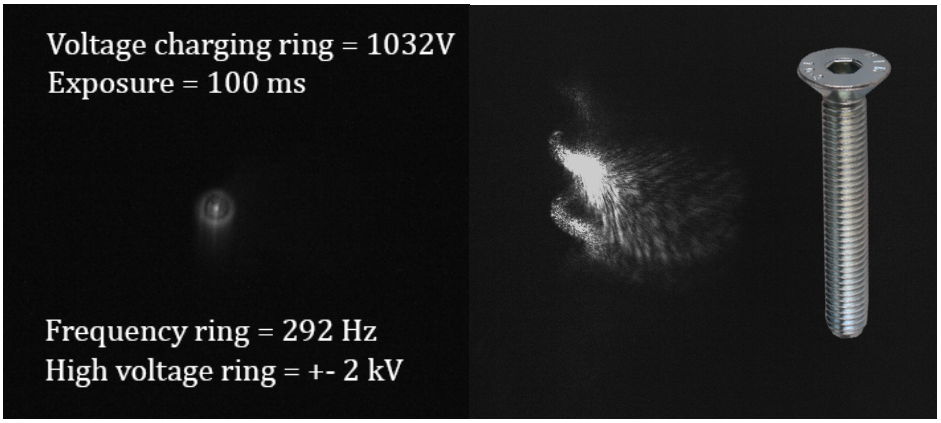

(a) **(b)**

Figure 4.5: (a) Image of a droplet flying bye. A droplet is deposited from a solution of pure H_2O mixed with an arbitrary amount of kitchen salt (NaCl). (b) A tiny bolt with a diameter of 2 mm is inserted inside the trap. The schematic nut at the side is inserted just for referencing. The contours of the bolt are clearly visible on camera. This is a proof of principle for the size calibration.

4.2 Discussion

The main question of this thesis is aimed to study the behavior of a microdroplets during the process of evaporation and disintegration in ESI. Progress has been made to design an experimental setup that can study these aspects, however the ultimate goal of having a setup that can capture high resolution images of the molecular distribution within the droplet has not been reached. This discussion will analyze the steps that have been made toward such an experiment. The next chapter will elaborate on this discussion by describing the design of an ideal setup, based on the lesson learned from this research. As a basis for the discussion we will use the main question and sub-goals to analyze the current position of the experiment. These goals were described and substantiated in section 1.1. Here we will discuss the progress made for each goal:

main-goal:
"How should we design an experiment in which we can study both the shape deformations and molecular distribution within ionized microdroplets during the process of evaporation and disintegration."

sub-goals:

1. Can we use an quadrupole ion trap to trap and investigate small droplets at a fixed position in space?

2. How can the internal and external movement of molecules inside the droplet be studied during the process of ESI?

3. Can we confirm the known evaporation models with this experimental setup and determine the limits of applicability and limitations for these models?

4. What machinery do we need to study microdroplets with the resolution and detail necessary to unravel the evaporation models.?

It is clear that the main goal to study the behavior of microdroplets during the process of evaporations is not reached (yet). However the underlying theory and setup to accomplish this goals has been investigated and explored which lay a solid foundation for further understanding and experiments.

4.2.1 Sub-goal 1: Understanding the quadrupole trap

1. Can we use an quadrupole ion trap to trap and investigate small droplets at a fixed position in space?

In section 2.2 the mathematical theory of the underlying principle of the quadrupole ion trap has been presented. This theory has an exact solution that describe stable operation regions to trap a charged particle. This precise understanding has lead the widespread usage of quadrupole ion traps. Both theory and experiment show the working principle of this trap, however still the trapping of droplets is the main defect in this experiment. The ability to catch and maintain droplets in space is the very basis of this research.

It has been shown that charged grains of sand could be trapped in the center of the quadrupole trap. However there is no reproducible proof that droplets could be trapped in the center of this trap. Droplets have been captured flying through the trap with an repetition rate of 1 Hz. By adjusting the delay of the external trigger, images of these droplets could be captured on camera in the center of the trap. A clear influence of the oscillating potential applied to the ring was visible through the motion of the droplets. This implies that the droplets do contain charge that is affected by the potential inside the trap. However this did not lead to the desired result: trapping of the droplets.

The configuration of the quadrupole trap in combination with the grains of sand that have been trapped undoubtedly suggest that the solution to the problem of trapping the droplets lies in the interaction between the charge of the droplets and the potential field within in the trap. As a first step it could be investigated how the trap was used in the mass-spectrometer from which it was extracted. If there is information available about the size of the droplets and the potential applied to the trap inside this spectrometer, it could be used to establish why the trap is not working properly in this experiment.

This experiment is based on similar experiments that have been done where the shape deformation of the droplet during the Coulomb instability were studied [9]. There are two main differences if we compare the setup from [9] and the setup described in this thesis. The first difference is that E. Giglio et al. kept the ring electrode at ground potential and applied an oscillating potential to the top and bottom caps. This difference should not influence the stability of the droplets in the trap because it generates the same potential difference in the center of the trap. In the current configuration of this

experimental setup it is impossible to test this configuration because the top and bottom caps are electrically connected to the operating table.

Another difference lies in the construction and use of materials of the French trap. Their caps are made of highly conducting copper in comparison with our caps that have been made of an steel alloy. Depending on the type of steel, the conductivity can be a factor 10 larger for copper. The second constructive difference is that the trap used by E. Giglio et al. was a factor two smaller. It is well known that the potential generated by a point source scales inversely with the distance. In the experiment of E. Giglio et al. they applied a potential of ± 1500 V, while our maximum was ± 2000 V.

It seems that the potential-charge interaction of the droplets at the center of the trap reaches an limitation where the potential is not deep enough to attract the droplets to the center. To solve this problem the configuration could adapted so that 1. The droplets carry more charge or 2. The potential at the center of the trap is higher.

The first option has been tried during the experimental period by adding a salt to the solution (thus creating more ions in the solution) and by increasing the bias on the ring electrode through which the droplets move before entering the center of the quadruple ion trap. Both changes did not lead to the significant improvement of trapping the droplet. The increase in the voltage of the ring electrode reached a limit at $\sim \pm$ 6kV where to potential was so high that sparks skipped between the ring and the top cap of quadrupole trap. The adding of a salt, or more general adding of ions did not only lead to no significant change, it is highly undesirable to change the composition of the solute. This can lead to potential restrictions in choosing your solvent or molecules that you want to study because of their compatibility with the ion source in the solution.

The second option is to increase the potential inside the trap. Firstly the conductivity of the material should only influence how fast the potential inside the trap is established. A lower conductivity would lead to a higher resistance, but not to a lower final potential of the trap as we will see in the section below. Although the conductivity of the used materials differ greatly, both are highly conducting materials. Because of this it is very unlikely that this will influence the final potential inside the trap at the relatively low oscillating frequencies that are used in this experiment. It was tested if the amplifier had enough power to put the ring at a bias. This did not impose a limitation for the working of the trap.

A final proposed solution to reach an higher potential in the center of the used trap is to increase the overall potential applied to the trap. At the moment this is limited by the amplifier that generates the oscillation high voltage. Increasing this high voltage would also increase the potential at the center.

Numerical simulations

Calculating the potential can be a difficult and tedious task for non standardized objects. However the geometry of the quadrupole trap is relative simple and exact solutions for describing the potential inside the trap are availably. The optimal configuration of the quadrupole ion trap has no disruptions in its shape and the ratio between z_0 and r_0 is given by: $r_0^2 = 2z_0^2$ [50] (shown in figure 4.6. The parameters of the current trap are: $r_0 = 10$ mm, $z_0 = 7.4$ mm which is not exactly the optimal theoretical ratio (Using $r_0 = 10$ mm, z_0 should be 7.07 mm). To check the established potential for the modified ring we have done a simulation in COMSOL Multiphysics to calculate the static potential. The model of the ion trap is shown in figure 4.7.

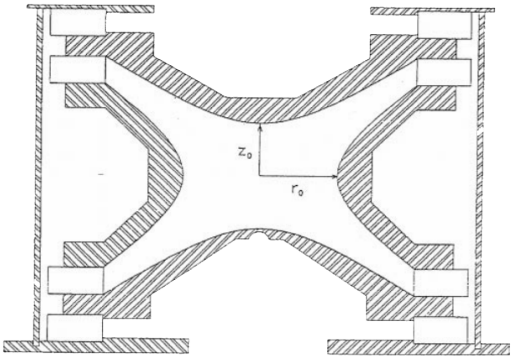

Figure 4.6: A cross section of the quadrupole ion trap showing the r_0 and z_0 parameters. Picture copied from [50].

Several different numerical studies have been done:

1. A static potential of ±2000V on the ring electrode while the caps are kept at ground potential.

2. A static potential of ±2000V on the caps while the ring electrode is kept at ground potential.

As expected, the outcomes of the above numerical studies are very similar. In fact they are exactly identical to each other with some trivial unitary sign translation. This is shown in the figure 4.8.

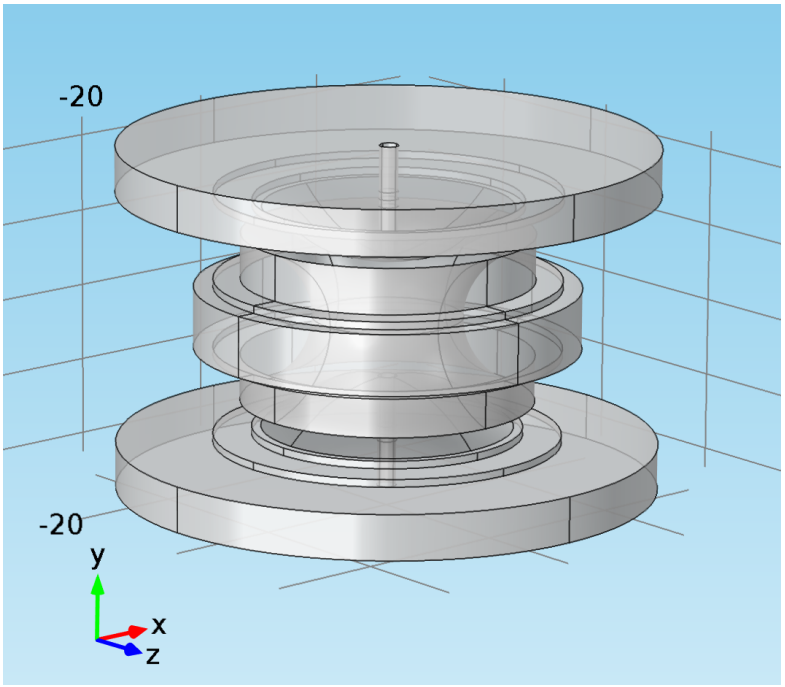

Figure 4.7: Model of the quadrupole ion trap as build in COMSOL Multiphysics version 4.3a. The corrugated spacers have been neglected in this model

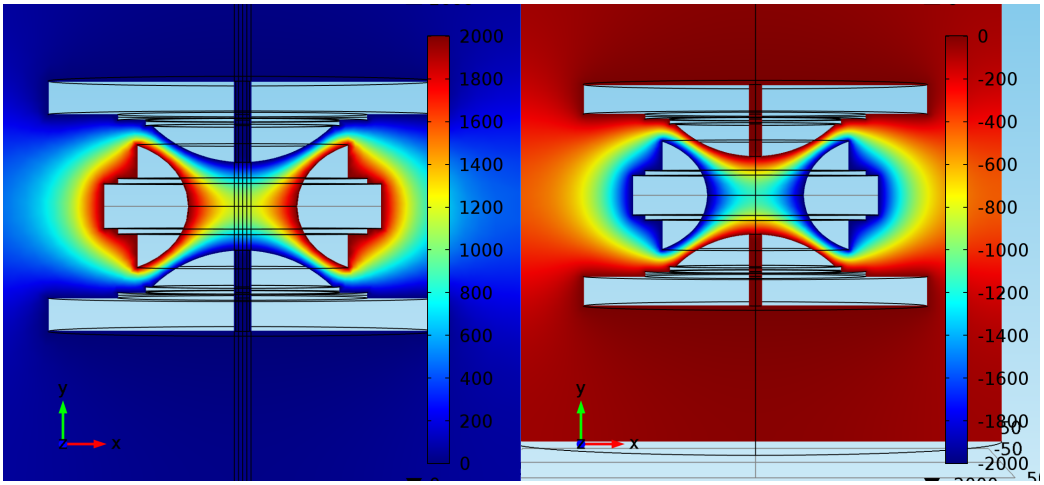

(a) Ring electrode = +2000V **(b)** Ring electrode = -2000V

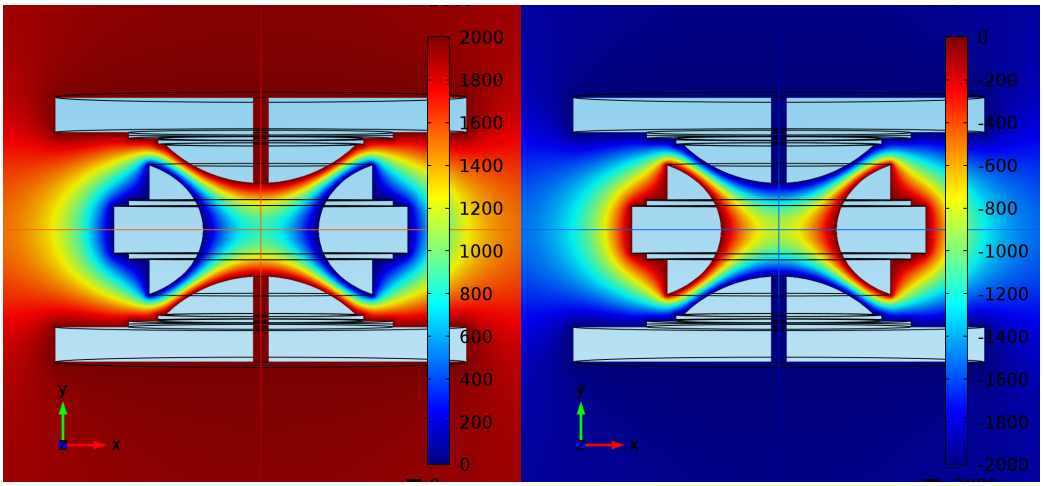

(c) Caps = +2000V **(d)** Caps = -2000V

Figure 4.8: Cross sections of the quadrupole trap in the XY-plane trough the center of the trap (figure 4.7). All figures are generated with COMSOL Multiphysics version 4.3a and represent the static potential in and around the trap. Because of circular symmetry, this image gives all the information of the 3D potential in the trap.

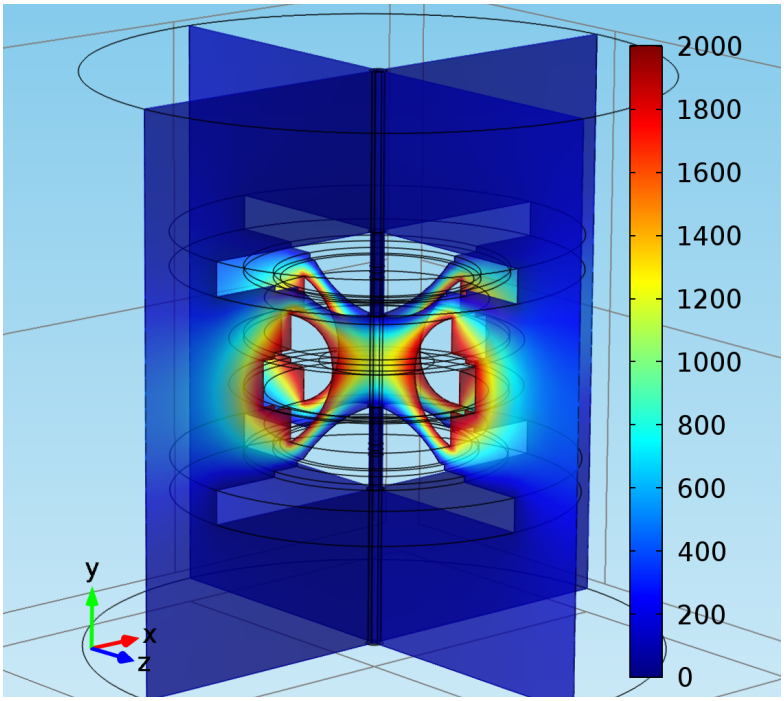

Figure 4.9: 3D representation of figure 4.8a where the full quadrupole outline is visible.

We can plot the potential in a 2D graph along a certain line. We have defined a line perpendicular to the X-axis going through the original of the X-axis. The resulting plots are shown in figure 4.10. As expected from the previous graphs, the figures are inversely identical.

A second numerical study is done when the trap is half the size of the trap we used in this experimental setup. Every size parameter is scaled down by a factor of two, but the potential parameters are kept constant. Again we have the circular symmetry that can map every potential configuration from the previous numerical study onto each other. Therefore only one study is done for this configuration: ring electrode = +2000V and the caps are kept at ground potential. The resulting line plot of the potential parallel to the X-axis through the origin is plotted together with the results from the simulation for the trap of the experiment. The results are shown in figure 4.11.

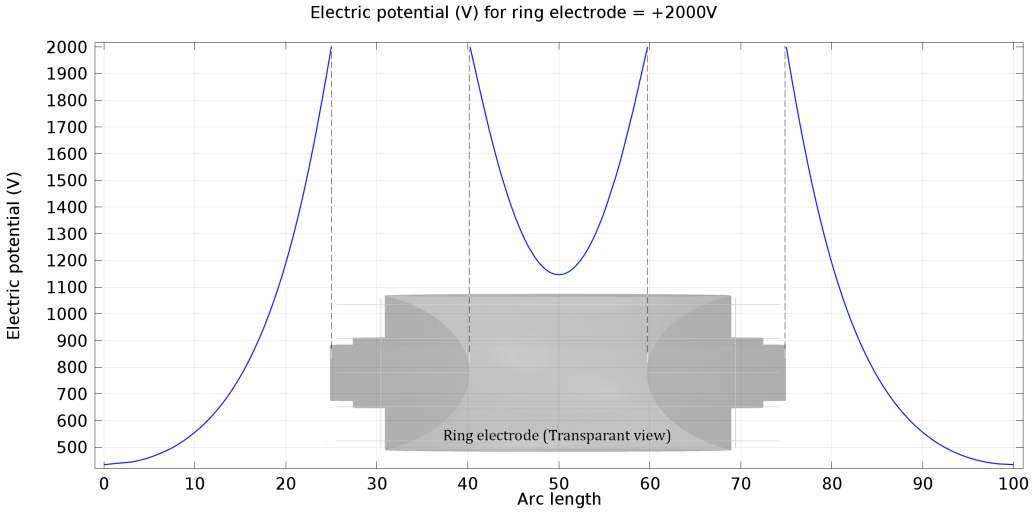

(a) 2D plot along a line perpendicular to the X-axis though the origin when the potential of the ring electrode = +2000V

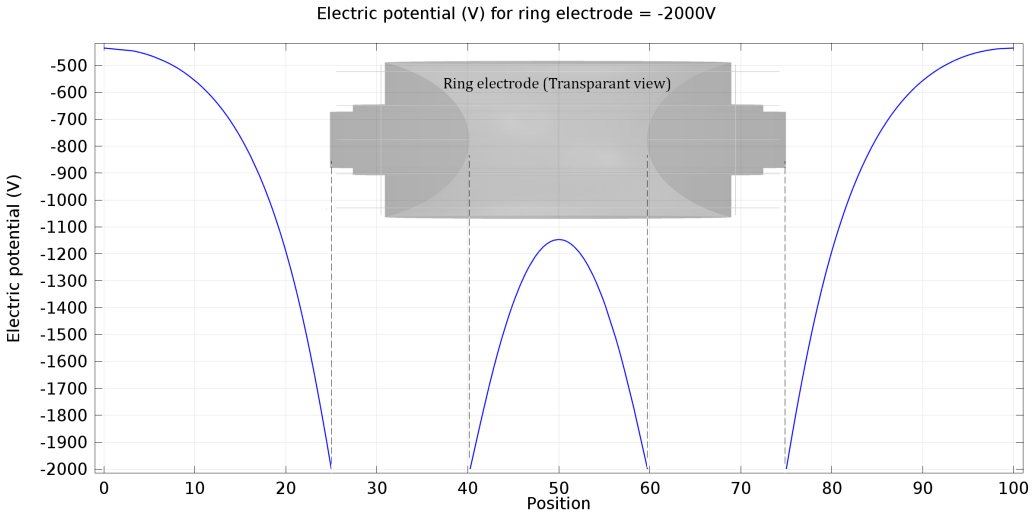

(b) 2D plot along a line perpendicular to the X-axis though the origin when the potential of the ring electrode = -2000V

Figure 4.10: Plots of the numerical simulated potential within the quadrupole ion trap. A schematic view of the toroidal ring of the quadrupole trap is placed inside the plot. From this it should be clear where the potential is located in space. We see that there is an local minimum and maximum at the center of the trap.

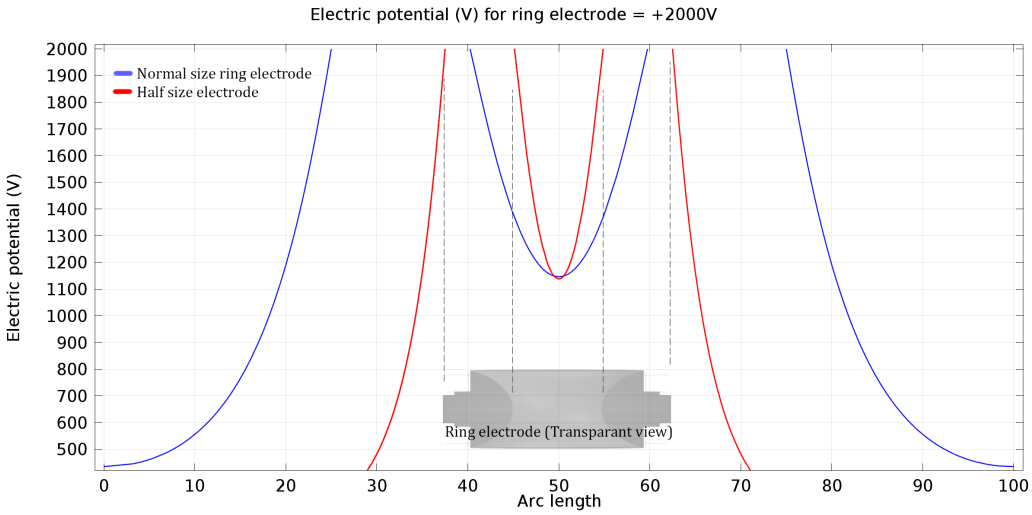

Figure 4.11: Numerical simulated comparison of the static potential of the quadrupole trap used in the experiment and a theoretical trap half the size. The trap inside the figure corresponds to the later one.

From the simulation it is clear that the absolute height of the static potential in both cases is approximately 1150V which is an intuitively expected answer based on the theory of calculating potentials at a distance [51]. Although the shape of both potential is similar, the potential well of the smaller trap is much more narrow.

A second aspect that still needs to be considered for this simulation is that it is a static one, not a dynamic simulation. We actually need to consider the potential dept established by the oscillating bias to compare the two traps quantitatively. To make this comparison we calculate the time-averaged (pseudo) potential dept inside both traps. The pseudo potential model is a approximation for the time independent potential dept in time dependent systems [52].

According to [52], the time-averaged (pseudo)potential dept in the axial and radial direction are given by:

$$\bar{D}_z = \frac{QV_0^2}{4Mz_0^2\Omega^2} \tag{4.1}$$

$$\bar{D}_r = \frac{QV_0^2}{4Mr_0^2\Omega^2} \tag{4.2}$$

Where Q is the total charge, M is the total mass of the particle. For Q we will use the charge measured by [9] which is 3.3 pC. Comparing the parameters from this experiment (V_0 = 2000V, r_0 = 10mm, $\Omega = 2\pi$f, f= 200 - 7000 Hz, $M = 2.14 * 10^{-9}$ kg (based on a water droplet, diameter of 80 μm)) with the parameters from [9] (V_0 = 1500V, r_0 = 5mm, $\Omega = 2\pi$f, f= 200 - 1000 Hz,$M = 6.43*10^{-11}$ kg (based on a glycol droplet, diameter of 24 μm)).

The resulting potential depths are listed in the table below:

	Quadrupole trap		Quadrupole trap used by [9]	
	$\bar{D}_z$ (V)	$\bar{D}_r$ (V)	$\bar{D}_z$ (V)	$\bar{D}_r$ (V)
Bottom: 200 Hz	19.5	9.77	1463	731
Top: 1000 Hz	0.781	0.390	58.5	29.3
Top: 7000 Hz	$1.59e^{-2}$	$7.95e^{-3}$	1.19	0.597

The potential dept determines the amount of kinetic energy which the ion inside the trap may acquire through resonant exciting (motion induced by secondary quadrupole trap effects) while still being kept stable inside the trap [53]. In our case we are interested if the pseudo potential dept is large enough to overcome the gravitational and kinetic energy of the initial falling droplets.

To deepen this potential a DC voltage U_0 could be applied to the top and bottom caps. If the voltage is applied symmetrically the new potential dept can be estimated with [52]:

$$\bar{D}'_z = \bar{D}_z + \frac{U_0 r_0^2}{2z_0^2} \tag{4.3}$$

$$\bar{D}'_r = \bar{D}_r - \frac{U_0 r_0^2}{2z_0^2} \tag{4.4}$$

From the potential dept calculations we can conclude that this potential is almost two orders of magnitude smaller for this experiment than for comparable successful experiments. It should be noted that this is not a quantitative comparison since more than one parameter is different in the calculation of the potential dept for both traps. However the calculated numbers do give insight in the difference between the traps. For further experiments the concept of potential depths and effective potential should be studied [54, 55]. A very nice approach to the determination of the optimal parameters can be found in [52]

4.2.2 Sub-goal 2: Movements of the molecules

2. How can the internal and external movement of molecules inside the droplet be studied during the process of ESI?

In section 2.3 and 2.4 the processes of fluorescence and the mathematical basis for an Abel transform has been presented. A camera to capture images and a laser to excite the fluorescent molecules as described in section 3.3 should be able to track the molecules inside the droplet. Estimates of the fluorescent lifetime show that the initial droplets emit enough photons to be detected. A simple experiment can be done to test if the fluorescent molecules inside the microdroplets can be tracked. By making use of the microdroplet dispenser camera to image droplets directly under the droplet dispenser and illuminating them with the laser it should be able to detect the fluorescent molecules. Shielding all incoming light and placing a proper filter between the droplets and the camera will results in only imaging the fluorescent photons.

The resolution of the images captured by the CCD-camera are limited by the number of photons emitted in a predefined time-frame and the number of pixels on the camera. The time-frame will define temporal resolution and thus correlates with the movement of the droplet. The number of pixels in the camera determine the details that will be captured. But on the other hand, larger resolution of the camera also means that more photons are needed for a good, but more detailed signal.

We can make a rough estimate of the number of molecules that end up at the CCD-camera. For this we have to make some assumptions for the efficiency parameters, however most have a linear relation with the results, so that it is intuitively clear what the change in estimated parameter will be on the end result. We will do this calculation for droplets of sizes between 40 and 75 μm. We first calculate the size of the droplets, then we assume that 1% of these droplets are made up of fluorescent molecules. By making use of the density and Avogadro's number we can calculate the number of NBD-Cl molecules in the droplets (table below, column 4). Finally by assuming that the fluorescent molecules are emitted in all directions and only the molecules passing through the 2 mm opening in the ring electrode at a distance of 10 mm reach the camera we end up with the number of photons at the camera.

There are two final corrections we need to do: first we need to correct for the quantum efficiency of the camera (the fraction of photons that is actually converted to a signal) which is 40% and the fluorescence quantum yield for NBD-Cl (the number of molecules that exhibit fluorescence per photon absorbed) which is 1% at its highest according to [56].

Finally we need to calculate the number of photons provided by the laser. We know the wavelength and power of the laser (450 nm and 4.5 mW) which can be convert to the energy per photon for this wavelength. Dividing the power by this number we come to the answer that approximately 1.02e16 photons hit the droplet per second if the laser is fully focused on the droplet.

	Volume (m^3)	Mass (NBD-CL)	Molecules	Photons at camera
40 μm	2.6808e-15	4.5842e-12 kg	1.3834e13	1.3834e09
75 μm	1.7671e-14	3.0218e-11 kg	9.1192e13	9.1192e09

Using the quantum efficiency and fluorescence quantum yield we end up that for approximately 5.5337e6 - 3.6477e7 photons reach the detector for droplets between the size of 40 and 75 μm respectively, for each excitation of the fluorescent molecules. The laser provides a saturated amount of photons to the droplets, however this is not calculated since it is not straightforward how many photons are excited each second by the laser beam. Furthermore CCD-cameras can potentially detect single photons (not taking the quantum efficiency into account) and therefore this estimate concludes with the notion that enough photons reach the detector to generate a image.

Reproducibility of the exact droplet at the exact same circumstances could improve the resolution because multiple measurements can be added to end up with a very clear image of the droplet. In situ measurements will reveal the actual captured images and the resulting resolution. To conclude this subgoal: the theoretical underlying principles have been sufficiently studied for this experiment, and in further experiments it could be checked if we indeed are able to track fluorescent molecules inside the droplet.

4.2.3 Sub-goal 3: Evaporation models

3. Can we confirm the known evaporation models with this experimental setup and determine the limits of applicability and limitations for these models?

Section 2.5 has listed the currently known evaporation models. It concludes with the remark that every models is valid within their respective boundary conditions. This last statement points out that the actual processes at work are still not well understood, which is remarkable for an process on which large industries rely for their operation. It also shows that there is an opportunity to do significant discoveries and develop models that are applicable within the whole range of molecular parameters.

Currently there is not one model that is widely accepted for all applications and the most recent research by Leisner et al. or E. Giglio et al concludes that there is a discrepancy between their theoretical modulations and their observations. There is room and need for the development of new models. Building on the current models, the development of new models can be done by making use of results of precise molecular distribution experiments such as the experiment described in this thesis.

4.2.4 Sub-goal 4: Extra apparatus needed

4. What machinery do we need to study microdroplets with the resolution and detail necessary to unravel the evaporation models.?

The current setup is describe in chapter 3 and the results are listed in the first section of this chapter. During the development of this experimental setup lessons have been learned and several trapping parameters have been investigated to learn how the experimental setup works and is operated. The possible improvements and expansions of this experiment have become a great point of interest for this research and therefore the next chapter is devoted to designing the ideal experiment. In this chapter the absolutely necessary improvements and possible additions to the experiment are discussed.

4.2.5 Motivation for this research

The motivation of this research was explained in the introduction of this thesis. Now at the end of this research and thesis, the motivation should be reevaluated and cross-checked with possible practical applications.

A pure scientist is driven by the gain in knowledge of the most fundamental processes around us. Guided by this reason to do research, this research could have a large success-rate because it can give insight in processes that are currently poorly understood. Sadly the current society does not leave a lot of room for the fundamental search to understand the world around us and luckily this research can also offers new knowledge and insights that has direct applications. In sections 1.1 and 2.1 it is described what the current applications of ESI are. A multi-billion dollar industry relies on this specific process and most obviously is interested in the improvement of the technique.

Advances in the understanding and theory of this evaporation process has both scientific and industrial interest and therefore the continuation of effort to improve and expand this experiment should be secured by additional (financial) sponsors. This conclusion is reached basing the arguments only on the direct industrial applications, and considering the scientific value as a bonus of this research.

Chapter 5

Further experiments

"Science is curiosity, testing and experimenting."

— Venkatraman Ramakrishnan

Up to this point, no droplets have been successfully trapped and analyzed inside the quadrupole trap. This experiment has been proposed because it is thought that the study of these evaporating droplets has both scientific and industrial value. At the moment of writing the literature does not give an unambiguously answer to describe the process of evaporation and disintegration for the process of electrospray ionization. Therefore it can be concluded that experiments to study this process remain a point of interest.

Lessons have been learned from building and troubleshooting the experimental setup and this newfound information is used to write this chapter. In the first place, the aim of this chapter is to describe improvements that can be made to the experimental setup so that the microdroplets can be studied.

This chapter does not take the financial aspect into account, it aims to describe the ideal setup that can study several aspects of the droplet evaporation process. It describes essential improvement to make the setup work, and secondly it describes possible enhancements of the setup through which an range of interesting other properties of the microdroplets that possible have a role in the evaporation process can be studied.

5.1 Essential improvements

5.1.1 Quadrupole trap

Redesigning the trap to decrease the distance between the central ring, caps and the center of the trap definitely lead to an increase in the potential dept at the center of the trap. With the redesign of the trap it should be carefully studied what the effect of holes in the ring electrode are on the resulting potential at the center of the trap. These holes possible lead to disruptions in the radial potential distribution of the trap. A smaller trap means that holes of the same diameter (2 mm) cause a relatively larger disruption in the potential. Redesigning the trap has some additional advantages, the material can be chosen, the amount of material can be optimized (thus minimizing the resistance), and even the machinery that needs to be attached to trap can be taking into account at the redesigning to make it fit perfectly and eliminate tedious aligning tasks.

5.1.2 Imaging of droplets

If the challenge to trap droplets inside the quadrupole trap is overcome and droplets can be captured and kept at the center of the trap, imaging the droplets becomes the next big challenge. To study the molecular distribution of dissolved analyte in the droplet it is absolutely vital to capture a clear images of the droplet. It is determined that the specifications of the current camera match the requirements. This is mainly determined by the shutter time of the camera, the exposure time, the resolution and te quantum efficiency.

The CCD-camera has a lens mounted that can be adjusted to focus onto the droplet. However the preliminary results show that steps can be made to increase this magnification. The experiment used separate lenses that were at hand to magnify the droplet, and the CCD-camera lens was used to focus this image. In the images captured less than 1% of the image consisted of the droplet. Additional magnification could increase the droplet projection on the images taken with the CCD-camera. It is found that the focusing of the droplet using the lensing system is a tedious and time-consuming task with marginal results. An microscope objective with the right focal point, mounted on an holder that is attached to the quadrupole trap could provide a solution to these magnification problems.

The second point that needs to be considered is that the number of photons that reach the camera might become an limitation. The images from the results show that there is an saturation when there is no fluorescence imaging filter in place. All the photons that reach the camera are generated by the laser and reflected from the droplet.

A quick estimate on the number of photons that reach the camera is done. In section 4.2.2 and although it relies on assumptions it is concluded that the photons emitted from the droplet do not impose a limitation on the images that will be taken from the droplets.

However during the time resolved analysis of the droplet, the droplets will evaporate and less fluorescent photons will be present in the smaller droplets. The actual limit of this has to be estimated after in situ measurements have been done and the actual number of photons reaching the detector are measured. To studying the shape of the droplet can be achieved by installing a flash-lamp, an very intensive stream of photons that illuminates the droplet in the nanosecond range, and creating the ability to track the droplet during the process of evaporation, effectively capturing the shadow of the droplet. This addition does only aid the tracking of droplets and does not improve the fluorescence. The maximum fluorescence of a single droplet is inherently connected to the number of fluorescent molecules and can therefore only be increased by increasing the concentration of fluorescent molecules. Though if individual droplets can be exactly reproduced, repeating the process with the same parameters, the intensity of several images could be combined to result in one image where the average position of the molecules can be tracked within the small droplet.

5.2 Improvements and enhancements

After considering the essential improvement to image the fluorescence of the analyte inside microdroplets it is worth investing some time to consider what other enhancements can be made to maximize the yield of this experiment. This section is devoted to discuss the possible improvements or enhancements that can be made to the experimental setup. These improvements are based on similar experiments [8, 9] and the operation, building and testing of the experimental setup of this thesis.

5.2.1 Improvements

Alignment and vibrations: The experimental setup has been build and rebuild several times to improve the alignment. The laser is focused and has to go through the center of the trap. At the same time the camera has to be exactly perpendicular to this laser, focused on the second hole in the toroidal central ring of the quadrupole. This aligning has been a tedious and precise task, especially when new elements such as lenses or diaphragms were places in the setup.

The whole setup would greatly benefit if the trap and the elements that are directly related to the imaging of the droplets are placed in a frame that is design for this. This not only eases the building an operation, it also increases the reproducibility of experimental configurations.

Having a robust frame to build on, this will have as a additional benefit that the whole setup is more stable. Vibrations in the system were very visible during the operation. Movements of the experimental table translated to blurry images. The reproducibility is very important because the experiment relies on the fact that subsequent droplets are assumed to follow the same path of evaporation. Having a firm and solid frame on which all the elements are mounted can remove some of the vibrations and misalignment that are present if the parts are mounted individually.

Droplet dispenser: Reproducibility of the droplets is key to this experiment. The operation of this dispenser head brought some challenges to the experiment. The manual filling, flushing and emptying of the dispenser head made it a prerequisite for the setup that the dispenser head was adjustable and removable. As a result it took a lot of time to align the dispenser head so that droplets emerging from this head reached the center of the quadrupole trap. It was also found that the angle from which the stream of droplets emerged from the dispenser head varied in time, and therefore the position and angle of the dispenser head had to be calibrated before each use. Having a dispenser head that does flushing of the fluid automatically and releases the droplets straight down from the dispenser head without an angle would resolve this problem. A droplet dispenser that deposits a steady straight steam of droplets that remain constant during (intensive) operation of the dispenser head would be perfect for this experiment .

5.2.2 Enhancements

Height control and Feedback loop: The enhancement of height control stems from a similar experimental setup that also required the stabilization of droplets in space [9]. As described in section 2.2 we apply an oscillating potential with an possible superimposed DC potential to the ring electrode. In our setup we neglected the DC-potential because we assumed that the oscillating potential would deep and fast enough to capture the droplet. Adding a feedback loop where the droplet in the trap is monitored and the height information is used to change to DC potential to stabilize the height op the droplet could enhance the stable and lengthy operation of the experiment.

The reflections of the droplet should be projected on a vertical CCD-array which then directly translates to the height of the droplet. In a feedback loop, a change in height should correspond to an change in the imposed DC potential on the caps of the quadrupole trap. As an additional advantage, the monitoring of the droplet could also be used to trigger the camera. The Coulomb instability could be seen by the change in reflection pattern on the CCD-array and thus triggering the camera. An adjustable delay would match directly to the stage of the Coulomb fission process. It is noted that the droplet instability could also be monitored with a single diode, not having the height control, but only the trigger control. In both cases, with or without an array, the diode(s) should be sensitive enough to detect changes from the scattering of light from the droplet.

Temperature control: To maximize the controllability and reproducibility of the experiment it should be possible to carefully manage the temperature and ambient conditions inside the trap. Extraction of the droplet has to be done at ambient conditions, however the droplet can be transfer to a (medium) vacuum environment where it is thermally insulated from ambient conditions. By placing only the trap inside a vacuum chamber while leaving the droplet dispenser above it, it is possible to create a medium vacuum. Adding a cryostat can be used to control the temperature

Flash-lamp: A flash-lamp provides a brief, sudden burst of photons that illuminates the droplet intensely. This flash-lamp effectively does the same as the exposure time of the camera. However this flash-lamp provides a high amount of photons that lead to a sharp projection of the shadow of the droplet that can be captured by the CCD-camera. This technique of capturing the shadow is called shadowgraphy. Because this burst of light has a much shorter timespan than the processes at work in a evaporating droplet

it can be used to capture certain stages of the evaporation and disintegration process of the droplet. This flash-lamp only aids if the minimum exposure time of the camera does not capture enough photons to display clear droplets. It is noted that this flash-lamp would aid resolving the shape deformations exhibited by the droplet, but generally does not help to resolve the molecular distribution of the molecules inside the droplet because it does not trigger fluorescence. It could trigger fluorescence if the wavelength of the photons of the flash-lamp matches the excitation wavelength of the fluorescent dye. Although very unlikely, it could be possible that this combination of wavelength and dye is availably.

At this point it is assumed that the size and charge of the molecules in the droplet determines the fission behavior, this can be derived from the Rayleigh limit given in equation 2.1. It would be interesting to study the fission behavior of these droplets as a function of the charge they carry. It is likely that the shape deformations of the droplets are influenced by the charge inside and at the surface of the droplet. By analyzing the scattered light it is possible to determine the mass over charge ration. Precisely composition of the solution and size determination of the imaged droplets make it possible to resolve the total charge on each droplet.

5.3 Ideal experiment

The points mentioned in the discussion- and previous section have been combined in a schematic overview of the ideal experiment shown in figure 5.1. This schematic is created by adapting the initial design which contains the quadrupole ion trap and some imaging apparatus. compared to this basic experiment there have been some additions to the machinery. In the ideal experiment there is an flash-lamp and an CCD-array present, working as described in the previous sections. The CCD-array is necessary for an precise height control of the droplet and the flash-lamp is to have collect shadowgraphy images of the droplets.

Besides the proposed changes that can directly been seen from the schematic setup, there are two major additional propositions to adapt the experiment. First of all the quadrupole ion trap should be modified so that the potential dept at the center of the trap is increased, and thus more easily trap moving charged droplets.

Secondly, the stream of droplets should be deposited straight down from the droplet dispenser. The apparatus currently used has shown to produce droplets with a high repetition and reproducibility rate, but the variable angle of the stream of droplets from the nozzle is a problem for the repeatability and execution of this experiment. Ideally we would like to use a nozzle that sprays droplets straight down without an angle, a stream that has rotational symmetry where the center aligns with the center of the droplet dispenser. This property can be used to design a holder which automatically aligns the position of the droplet dispenser to the ion trap. In this ideal experiment the dispenser head is replaced by a version that deposits the droplets straight down into to the quadrupole trap.

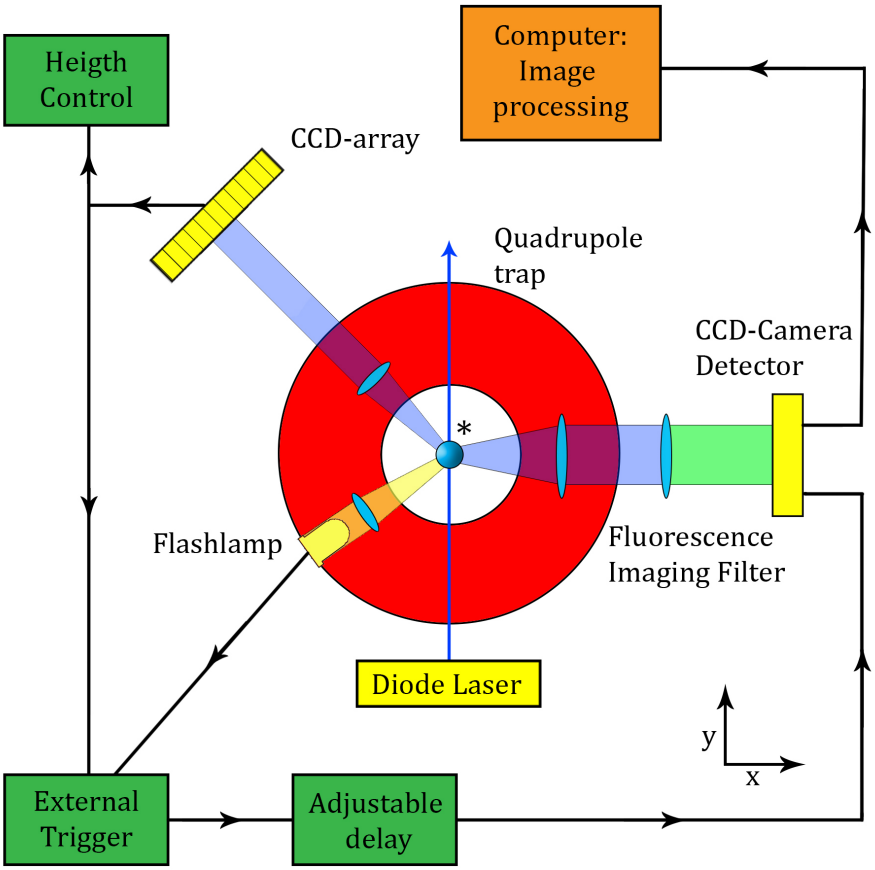

Figure 5.1: Schematic drawing of the ideal experimental setup, containing a flash-lamp and CCD-array (Schematic made by assuming a cross section through the horizontal plane of the quadrupole ion trap)

Bibliography

[1] Shibdas Banerjee and Shyamalava Mazumdar. Electrospray ionization mass spectrometry: a technique to access the information beyond the molecular weight of the analyte. *International journal of analytical chemistry*, 2012, 2012.

[2] Wolfgang Paul. Electromagnetic traps for charged and neutral particles. *Reviews of modern physics*, 62(3):531, 1990.

[3] Sabine Becker. *Inorganic mass spectrometry: principles and applications*. John Wiley & Sons, 2008.

[4] Gary Siuzdak, MCC Press, and Christoph A Schalley. The expanding role of mass spectrometry in biotechnology. *Journal of American Society for Mass Spectrometry*, 15:625, 2004.

[5] Alma Lyman Burlingame. *Biological mass spectrometry*, volume 402. Gulf Professional Publishing, 2005.

[6] L Boschman, G Reitsma, S Cazaux, T Schlathölter, R Hoekstra, M Spaans, and O Gonzalez-Magana. Hydrogenation of pah cations: A first step toward h2 formation. *The Astrophysical Journal Letters*, 761(2):L33, 2012.

[7] Lars Konermann, Elias Ahadi, Antony D Rodriguez, and Siavash Vahidi. Unraveling the mechanism of electrospray ionization. *Analytical chemistry*, 85(1):2–9, 2012.

[8] Denis Duft, Tobias Achtzehn, Rene Müller, Bernd A Huber, and Thomas Leisner. Coulomb fission: Rayleigh jets from levitated microdroplets. *Nature*, 421(6919):128–128, 2003.

[9] E Giglio, B Gervais, Jimmy Rangama, B Manil, Bernd A Huber, D Duft, R Müller, T Leisner, and C Guet. Shape deformations of surface-charged microdroplets. *Physical Review E*, 77(3):036319, 2008.

[10] Geoffrey Taylor. Disintegration of water drops in an electric field. In *Proceedings of the Royal Society of London A: Mathematical, Physical and Engineering Sciences*, volume 280, pages 383–397. The Royal Society, 1964.

[11] Nadja B Cech and Christie G Enke. Practical implications of some recent studies in electrospray ionization fundamentals. *Mass Spectrometry Reviews*, 20(6):362–387, 2001.

[12] Arthur T Blades, Michael G Ikonomou, and Paul Kebarle. Mechanism of electrospray mass spectrometry. electrospray as an electrolysis cell. *Analytical chemistry*, 63(19):2109–2114, 1991.

[13] Georg Diehl and Uwe Karst. On-line electrochemistry–ms and related techniques. *Analytical and bioanalytical chemistry*, 373(6):390–398, 2002.

[14] Richard B Cole. *Electrospray and MALDI mass spectrometry: fundamentals, instrumentation, practicalities, and biological applications.* John Wiley & Sons, 2011.

[15] Michael G Ikonomou, Arthur T Blades, and Paul Kebarle. Electrospray mass spectrometry of methanol and water solutions suppression of electric discharge with sf6 gas. *Journal of the American Society for Mass Spectrometry*, 2(6):497–505, 1991.

[16] Arno Wortmann, Anna Kistler-Momotova, Renato Zenobi, Martin C Heine, Oliver Wilhelm, and Sotiris E Pratsinis. Shrinking droplets in electrospray ionization and their influence on chemical equilibria. *Journal of the American Society for Mass Spectrometry*, 18(3):385–393, 2007.

[17] Lord Rayleigh. London, edinburgh, dublin philos. *Mag. J*, 44:184, 1882.

[18] Ulrich Brosa, Siegfried Grossmann, and Andreas Müller. Nuclear scission. *Physics Reports*, 197(4):167–262, 1990.

[19] F Chandezon, S Tomita, D Cormier, P Grübling, C Guet, H Lebius, A Pesnelle, and BA Huber. Rayleigh instabilities in multiply charged sodium clusters. *Physical review letters*, 87(15):153402, 2001.

[20] Keqi Tang and Alessandro Gomez. On the structure of an electrostatic spray of monodisperse droplets. *Physics of Fluids (1994-present)*, 6(7):2317–2332, 1994.

[21] Michele A Kelly, Martha M Vestling, Catherine C Fenselau, and Philip B Smith. Electrospray analysis of proteins: A comparison of positive-ion and negative-ion mass spectra at high and low ph. *Organic mass spectrometry*, 27(10):1143–1147, 1992.

[22] Paul Kebarle and Udo H Verkerk. Electrospray: from ions in solution to ions in the gas phase, what we know now. *Mass Spectrometry Reviews*, 28(6):898–917, 2009.

[23] Nelson P Barrera, Natalie Di Bartolo, Paula J Booth, and Carol V Robinson. Micelles protect membrane complexes from solution to vacuum. *Science*, 321(5886):243–246, 2008.

[24] Dayin Lin, David L Tabb, and John R Yates. Large-scale protein identification using mass spectrometry. *Biochimica et Biophysica Acta (BBA)-Proteins and Proteomics*, 1646(1):1–10, 2003.

[25] Vicki H Wysocki, Katheryn A Resing, Qingfen Zhang, and Guilong Cheng. Mass spectrometry of peptides and proteins. *Methods*, 35(3):211–222, 2005.

[26] Eugene Kolker, Roger Higdon, and Jason M Hogan. Protein identification and expression analysis using mass spectrometry. *Trends in microbiology*, 14(5):229–235, 2006.

[27] Yoshinao Wada. Advanced analytical methods for hemoglobin variants. *Journal of Chromatography B*, 781(1):291–301, 2002.

[28] CS Ho, CWK Lam, MHM Chan, RCK Cheung, LK Law, LCW Lit, KF Ng, MWM Suen, and HL Tai. Electrospray ionisation mass spectrometry: principles and clinical applications. *The Clinical Biochemist Reviews*, 24(1):3, 2003.

[29] Uma Krishnamurti and Michael W Steffes. Glycohemoglobin: a primary predictor of the development or reversal of complications of diabetes mellitus. *Clinical chemistry*, 47(7):1157–1165, 2001.

[30] Thomas PE Hollenbeck, Gary Siuzdak, and Robert D Blackledge. Electrospray and maldi mass spectrometry in the identification of spermicides in criminal investigations. *Journal of forensic sciences*, 44:783–788, 1999.

[31] Horst Elschner. Ein neues massenspektrometer ohne magnetfeld. *ZEITSCHRIFT FUR ANGEWANDTE PHYSIC*, 23(2):77, 1967.

[32] John Frederick William Herschel. No. i. on a case of superficial colour presented by a homogeneous liquid internally colourless. *Philosophical Transactions of the Royal Society of London*, pages 143–145, 1845.

[33] Joseph R Lakowicz. *Principles of fluorescence spectroscopy*. Springer Science & Business Media, 2013.

[34] Robert C Hilborn. Einstein coefficients, cross sections, f values, dipole moments, and all that. *arXiv preprint physics/0202029*, 2002.

[35] Life Technologies Corporation ThermoFisher. *NBD Chloride, 4-Chloro-7-Nitrobenz-2-Oxa-1,3-Diazole (4-Chloro-7-Nitrobenzofurazan) (FluoroPure™ grade)r*, 2013.

[36] Mark A Abramson, Thomas J Asaki, John E Dennis Jr, Kevin R O'Reilly, and Rachael L Pingel. Quantitative object reconstruction using abel transform x-ray tomography and mixed variable optimization. *SIAM Journal on Imaging Sciences*, 1(3):322–342, 2008.

[37] Vladimir Dribinski, Alexei Ossadtchi, Vladimir A Mandelshtam, and Hanna Reisler. Reconstruction of abel-transformable images: The gaussian basis-set expansion abel transform method. *Review of Scientific Instruments*, 73(7):2634–2642, 2002.

[38] RN Bracewell. The fourier transform and its applications: Mcgraw-hill book company. *New York*, 1978.

[39] Kjell Bockasten. Transformation of observed radiances into radial distribution of the emission of a plasma*. *JOSA*, 51(9):943–947, 1961.

[40] L Montgomery Smith, Dennis R Keefer, and SI Sudharsanan. Abel inversion using transform techniques. *Journal of Quantitative Spectroscopy and Radiative Transfer*, 39(5):367–373, 1988.

[41] Roberto Marchese, Rita Grandori, Paolo Carloni, and Simone Raugei. A computational model for protein ionization by electrospray based on gas-phase basicity. *Journal of the American Society for Mass Spectrometry*, 23(11):1903–1910, 2012.

[42] Christopher J Hogan Jr, James A Carroll, Henry W Rohrs, Pratim Biswas, and Michael L Gross. Combined charged residue-field emission model of macromolecular electrospray ionization. *Analytical chemistry*, 81(1):369–377, 2008.

[43] Elias Ahadi and Lars Konermann. Ejection of solvated ions from electrosprayed methanol/water nanodroplets studied by molecular dynamics simulations. *Journal of the American Chemical Society*, 133(24):9354–9363, 2011.

[44] Anthony T Iavarone and Evan R Williams. Mechanism of charging and supercharging molecules in electrospray ionization. *Journal of the American Chemical Society*, 125(8):2319–2327, 2003.

[45] Alan Fersht et al. Structure and mechanism in protein science, 1999.

[46] Denis Duft. *Laborexperimente zur Mikrophysik der Wolken*. PhD thesis, Universitätsbibliothek Ilmenau, 2011.

[47] Microdrop Technologies GmbH. *Microdispensing Sytem MD-E-3000 (Manual)*.

[48] Microdrop Technologies GmbH. *Microdispensing Dispenser heads (Manual)*.

[49] SDVision GmbH. *Sensicam Operating instructions*.

[50] Raymond E March. An introduction to quadrupole ion trap mass spectrometry. *Journal of mass spectrometry*, 32(4):351–369, 1997.

[51] David Jeffrey Griffiths and Reed College. *Introduction to electrodynamics*, volume 3. prentice Hall Upper Saddle River, NJ, 1999.

[52] Shenglan Qiao. *Constructing a Linear Paul Trap System for Measuring Time-variation of the Electron-Proton Mass Ratio*. PhD thesis, Amherst College, 2013.

[53] Günther Werth, Viorica N Gheorghe, and Fouad G Major. Charged particle traps ii. *Charged Particle Traps II: Applications, Springer Series on Atomic, Optical, and Plasma Physics, Volume 54. ISBN 978-3-540-92260-5. Springer-Verlag Berlin Heidelberg, 2009*, 1, 2009.

[54] Dieter Gerlich. Inhomogeneous rf fields: a versatile tool for the study of processes with slow ions. *State-selected and state-to-state ion-molecule reaction dynamics, part*, 1:1–176, 2007.

[55] R Otto, P Hlavenka, S Trippel, J Mikosch, K Singer, M Weidemüller, and Roland Wester. How can a 22-pole ion trap exhibit ten local minima in the effective potential? *Journal of Physics B: Atomic, Molecular and Optical Physics*, 42(15):154007, 2009.

[56] Biomol GmbH. Classic fluorescent labeling dyes, online page, https://www.biomol.com, visited on 2016-09-16.